

\mathcal{PT} -symmetry breaking in complex nonlinear wave equations and their deformations

Andrea Cavaglia^{*}, Andreas Fring^{*} and Bijan Bagchi[°]

^{*} Centre for Mathematical Science, City University London,
Northampton Square, London EC1V 0HB, UK

[°] Department of Applied Mathematics, University of Calcutta,
92 Acharya Prafulla Chandra Road, Kolkata 700 009, India

E-mail: andrea.cavaglia.1@city.ac.uk, a.fring@city.ac.uk, bbagchi123@rediffmail.com

ABSTRACT: We investigate complex versions of the Korteweg-deVries equations and an Ito type nonlinear system with two coupled nonlinear fields. We systematically construct rational, trigonometric/hyperbolic, elliptic and soliton solutions for these models and focus in particular on physically feasible systems, that is those with real energies. The reality of the energy is usually attributed to different realisations of an antilinear symmetry, as for instance \mathcal{PT} -symmetry. It is shown that the symmetry can be spontaneously broken in two alternative ways either by specific choices of the domain or by manipulating the parameters in the solutions of the model, thus leading to complex energies. Surprisingly the reality of the energies can be regained in some cases by a further breaking of the symmetry on the level of the Hamiltonian. In many examples some of the fixed points in the complex solution for the field undergo a Hopf bifurcation in the \mathcal{PT} -symmetry breaking process. By employing several different variants of the symmetries we propose many classes of new invariant extensions of these models and study their properties. The reduction of some of these models yields complex quantum mechanical models previously studied.

1. Introduction

One can adopt various points of view with regard to the usefulness of the study of complex classical and quantum mechanical systems. Being very orthodox one may just view the complex systems as providing a larger setting which allows a better insight from a broader framework when restricted to the real physical system. A very successful example for this viewpoint is the more than seventy year old proposal of the analytical S-matrix [1, 2], which is still pursued nowadays; especially in 1+1 dimensions. Genuinely non-Hermitian systems such as dissipative ones are also well studied, but they are usually regarded as open and are therefore not self-consistent [3]. In contrast, a more recent perspective allows

to regard certain complex quantum mechanical Hamiltonians also as perfectly acceptable self-consistent descriptions of physical systems [4], in the sense that they possess real energy eigenvalue spectra and well defined unitary time-evolution (see [5, 6, 7] for recent reviews). To consider pseudo/quasi Hermitian systems provides a very clear conceptual view in this respect as it makes use of a similarity transformation towards a Hermitian Hamiltonian system for which everything is well defined in a standard conventional sense, although such transformations do not exist for all types of such systems. A more radical view is to give a direct meaning to the non-Hermitian Hamiltonians without any reference to the Hermitian system. This latter point of view has to be taken in order to explain recent experiments in which non-Hermitian systems are studied on optical lattices, see e.g. [8], as the observed gain and loss can not be explained in a purely Hermitian setting. A further experimental realization has recently been proposed for graphene nanoribbons, where non-Hermitian Hamiltonians arise as effective Hamiltonians [9].

Largely inspired by the study of the quantum systems, also classical complex systems have been investigated recently. Naturally one may view them too in various ways, either as directly meaningful or only sensible when transformed to a real system. Many classical models have already been investigated from these various perspectives, such as complex extensions of standard one particle real quantum mechanical potentials [10, 11, 12, 13], non-Hamiltonian dynamical systems [14], chaotic systems [15] and deformations of many-particle systems such as Calogero-Moser-Sutherland models [16, 17, 18, 19]. These investigations led to new insights into the quantum theories based on the features found in these classical models, such as tunneling behaviour [13, 20], band structures [21] and even a complex generalizations of Bohr's correspondence principle has been formulated [22].

Extensions of field theories of nonlinear wave type, such as Korteweg-deVries (KdV) equations [23, 24, 25] and closely related models [26, 27, 28, 29] have also been investigated. These type of models will be the main subject of our investigations in this manuscript.

Pseudo or quasi-Hermiticity are often equivalent to a simultaneous parity and time reversal, so-called \mathcal{PT} -symmetry. Remarkably this property, or more general antilinear symmetry [30], of quantum mechanical systems is already visible on the classical level. It is known for more than fifty years that when this symmetry is unbroken the reality of the spectrum of the theory is guaranteed. *Unbroken* refers here to the property that

$$[\mathcal{PT}, H] = 0 \quad \text{and} \quad \mathcal{PT}\Phi = \Phi, \quad (1.1)$$

i.e. the Hamiltonian H is \mathcal{PT} -symmetric and its eigenfunctions Φ are also eigenstates of the \mathcal{PT} or any other antilinear operator. In case the latter property does not hold, one speaks of *spontaneously broken* \mathcal{PT} -symmetry and the eigenenergies become complex conjugate pairs. The \mathcal{PT} -symmetry can be broken spontaneously in two different ways, either by tuning some of the parameters of the models appropriately or by manipulating the domain on which the model is defined, see e.g. [31] for the latter possibility. One speaks of *broken* \mathcal{PT} -symmetry when neither of the relations in (1.1) hold. In this case one usually expects complex energies, but we will demonstrate in this manuscript that in some cases real energy spectra can be produced by breaking the spontaneously broken theory further in a controlled way.

Here we will trace these properties on the classical level and use the reality of the classical energy as a criterium to select physically meaningful complex models including their boundary and initial conditions. The role of Φ in (1.1) is in this case played by the solution of the classical field equation of motion, say $u(x, t)$. For a given Hamiltonian density \mathcal{H} depending on $u(x, t)$ the energy on the interval $x \in [-a, a]$ is computed by

$$E = \int_{-a}^a \mathcal{H}[u(x)] dx = \oint_{\Gamma} \mathcal{H}[u(x)] \frac{du}{u_x}. \quad (1.2)$$

Here and throughout the manuscript we use the standard convention $u_x \equiv du/dx$. When the system possesses periodic solutions, that is when $u(a) = u(-a)$ along a path Γ in the complex u -plane, we can employ the alternative contour integral version in (1.2). A simple argument [24] shows that the energy in the interval $x \in [-a, a]$ is guaranteed to be real if the symmetry property $\mathcal{H}^*[u(x)] = \mathcal{H}[u(-x)]$ holds for the Hamiltonian density. We will present here some unexpected examples of real energy solutions for which neither of the relations in (1.1) hold, i.e. the \mathcal{PT} -symmetry is broken for the Hamiltonian and the solutions.

Here we will investigate two different types of complexified wave equations. First of all we study in section 2 the most immediate way to complexify wave equations by introducing complex boundary values and initial conditions for the KdV-system. We investigate systematically the traveling wave and soliton solutions. We study complex trajectories in the complex plane of the KdV-field especially with regard to their properties under \mathcal{PT} -symmetry breaking. In section 3 we employ the different types of \mathcal{PT} -symmetry as a construction principle to propose new extended versions of the KdV-system. We investigate the new models in a similar fashion as their undeformed counterparts. Particular attention is paid to the question of what kind of conditions will lead to physical models, in the sense that they possess real energies. In section 4 we study the effect of complex boundary conditions and initial values on a nonlinear system with two fundamental fields coupled to each other, which is referred to as Ito system for some specific parameter choice. We also investigate the \mathcal{PT} -symmetry properties of these models. Due to the presence of an additional field when compared with the KdV-system we can identify four different versions of \mathcal{PT} -symmetry being realised in these systems, which we exploit in section 5 to construct new models. We study them from similar points of view as the previous ones. We draw our conclusions in section 6.

2. Complex Korteweg-deVries equation

Complex extensions of the KdV equation have been investigated already some time ago for instance in [32, 33, 34, 35]. However, \mathcal{PT} -symmetry has only been utilized recently in [23, 24, 25] in order to understand some of their properties and in particular to construct new models. The standard KdV system is known to be a Hamiltonian system with density

$$\mathcal{H}_{\text{KdV}} = -\frac{\beta}{6}u^3 + \frac{\gamma}{2}u_x^2 \quad \beta, \gamma \in \mathbb{C}, \quad (2.1)$$

leading to the Korteweg-deVries equation in the form

$$u_t + \beta uu_x + \gamma u_{xxx} = 0. \quad (2.2)$$

Usually the constants β and γ are chosen to be real, but here we allow them to take complex values, thus including the possibility for $u(x, t)$ to be complex. \mathcal{PT} -symmetry may then be realised in two alternative ways as

$$\mathcal{PT}_+ : x \mapsto -x, t \mapsto -t, i \mapsto -i, u \mapsto u \quad \text{for } \beta, \gamma \in \mathbb{R}, \quad (2.3)$$

$$\mathcal{PT}_- : x \mapsto -x, t \mapsto -t, i \mapsto -i, u \mapsto -u \quad \text{for } i\beta, \gamma \in \mathbb{R}, \quad (2.4)$$

both possibilities guaranteeing that $\mathcal{PT}_\pm : \mathcal{H}_{\text{KdV}} \mapsto \mathcal{H}_{\text{KdV}}$ holds. The underlying models respect one of the two symmetries and are therefore different as they correspond to two distinct choices of the coupling constant which may, however, be related by a simple rotation in u . Nonetheless, with regard to possible deformations to be discussed below this second symmetry allows to construct different types of new models.

A crucial feature of the model to be acceptable as physically consistent is the reality of the energy (1.2). In case of the Hamiltonian density \mathcal{H}_{KdV} the reality of the energy (1.2) is guaranteed for the two possibilities $u^*(x) = u(-x)$ when $\beta, \gamma \in \mathbb{R}$ or $u^*(x) = -u(-x)$ when $i\beta, \gamma \in \mathbb{R}$, resulting from \mathcal{PT}_+ or \mathcal{PT}_- , respectively.

2.1 \mathcal{PT} -symmetric, spontaneously broken and broken solutions

Let us now see which complex boundary conditions and initial values are physically permissible. In order to establish this, we first briefly recall how the traveling wave solutions of the KdV-equations of motion may be constructed systematically. Integrating (2.2) twice leads to the equation

$$u_\zeta^2 = \frac{2}{\gamma} \left(\kappa_2 + \kappa_1 u + \frac{c}{2} u^2 - \frac{\beta}{6} u^3 \right) =: \lambda P(u) \quad (2.5)$$

with integration constants $\kappa_1, \kappa_2 \in \mathbb{C}$ and $P(u)$ denoting a third order polynomial in u multiplied by an overall constant λ . A further integration yields

$$\pm \sqrt{\lambda} (\zeta - \zeta_0) = \int du \frac{1}{\sqrt{P(u)}}, \quad (2.6)$$

where we made the usual assumption that the field $u(x, t)$ acquires the form of a traveling wave $u(x, t) = u(\zeta)$ with $\zeta = x - ct$ and c denoting the wave speed. In complete generality this is an elliptic integral, but it is instructive to generate simpler solutions by systematically making some specific assumptions on the factorization of the polynomial $P(u)$. This solution method may then be extended to the deformed cases.

Demanding specific boundary conditions will impose further restrictions or might be entirely incompatible with certain factorizations of $P(u)$. For instance, in case we wish to implement vanishing asymptotic boundary conditions for u and its derivatives, the once integrated version of equation (2.2) and (2.5) implies

$$\lim_{\zeta \rightarrow \pm\infty} u, u_\zeta = 0 \quad \Rightarrow \quad \kappa_1 = \kappa_2 = 0. \quad (2.7)$$

In the following we will study the solutions in the complex u -plane. For this purpose it is useful to separate u into its real and imaginary part u^R and u^I , respectively, and decouple (2.5) into two first order differential equations in these variables

$$u_\zeta^R = \pm \operatorname{Re} \left[\sqrt{\lambda} \sqrt{P(u^R + iu^I)} \right] \quad \text{and} \quad u_\zeta^I = \pm \operatorname{Im} \left[\sqrt{\lambda} \sqrt{P(u^R + iu^I)} \right]. \quad (2.8)$$

In this set up we may then apply many of the techniques which have been developed for two dimensional dynamical systems, see for instance [36]. Most immediate is the application of the linearisation theorem at some fixed point u_f , converting the nonlinear system into

$$\begin{pmatrix} u_\zeta^R \\ u_\zeta^I \end{pmatrix} = J(u^R, u^I)|_{u=u_f} \begin{pmatrix} u_\zeta^R \\ u_\zeta^I \end{pmatrix}, \quad (2.9)$$

with Jacobian matrix

$$J(u^R, u^I)|_{u=u_f} = \begin{pmatrix} \pm \frac{\partial \operatorname{Re}[\sqrt{\lambda} \sqrt{P(u)}]}{\partial u^R} & \pm \frac{\partial \operatorname{Re}[\sqrt{\lambda} \sqrt{P(u)}]}{\partial u^I} \\ \pm \frac{\partial \operatorname{Im}[\sqrt{\lambda} \sqrt{P(u)}]}{\partial u^R} & \pm \frac{\partial \operatorname{Im}[\sqrt{\lambda} \sqrt{P(u)}]}{\partial u^I} \end{pmatrix} \Bigg|_{u=u_f}. \quad (2.10)$$

We denote the eigenvalues of $J(u = u_f)$ by j_1, j_2 . Provided the system (2.9) is simple and $\operatorname{Re} j_i \neq 0$ the linearisation theorem applies, stating that the phase portraits of the systems (2.8) and (2.9) are qualitatively the same in some neighbourhood of the fixed point u_f . The ten similarity classes for 2×2 -matrices fully characterizing all possible behaviours for the fixed points of (2.8) are reported for reference in appendix A.

2.1.1 Rational solutions

Factorizing $P(u)$ at first in the simplest way as $P(u) = (u - A)^3$ with one constant A leaves no freedom when solving (2.5), as all constants are fixed

$$\lambda = -\frac{\beta}{3\gamma}, \quad \kappa_1 = -\frac{c^2}{2\beta}, \quad \kappa_2 = \frac{c^3}{6\beta^2} \quad \text{and} \quad A = \frac{c}{\beta}. \quad (2.11)$$

Clearly asymptotically vanishing boundary conditions (2.7) are only possible for a static solution with $c = 0$. The evaluation of the expression (2.6) produces for this factorization the rational solution

$$u(\zeta) = \frac{c}{\beta} - \frac{12\gamma}{\beta(\zeta - \zeta_0)^2}, \quad (2.12)$$

with additional integration constant $\zeta_0 \in \mathbb{C}$. Taking ζ_0 as purely imaginary maintains the \mathcal{PT} -symmetry of the solution, whereas any real part may be compensated by a shift in ζ , which is kept to be real. Independently of the parameter choice, asymptotically all rational solutions of the type (2.12) end up at $\lim_{\zeta \rightarrow \pm\infty} u(\zeta) = c/\beta$, as we can also observe in figure 1.

Focussing at first on the \mathcal{PT} -symmetric scenario, we notice that while keeping the speed of the wave c real there are two possible choices for the conjugation leading to physical solutions, namely $u^*(\zeta) = u(-\zeta)$ when $i\zeta_0, \beta, \gamma \in \mathbb{R}$ or $u^*(\zeta) = -u(-\zeta)$ when $i\zeta_0, i\beta, \gamma \in \mathbb{R}$. We depict some complex trajectories in the u -plane in figure 1a for several

different initial conditions ζ_0 . We have taken the plus and minus sign in (2.6) for the upper and lower half plane, respectively. We observe that for a specific branch the point A in the u -plane appears to be either a stable or an unstable improper asymptotic fixed point. We adopt here the notion for the characterizations of fixed points from the linearisation (see appendix A for a classification), despite the fact that u_ζ is not a meromorphic function and the system is not easily linearized. This implies that only the choice with different branches for the upper and lower half will give rise to closed orbits as depicted. For increasing ζ , they run either out of the fixed point in the upper half plane and into it in the lower half or vice versa. The crossing of the trajectories with the real line is easily computed to be at $u(0) = c/\beta + 12\gamma/\beta(\text{Im}\zeta_0)^2$. This makes it evident that only complex trajectories may be closed, whereas the real solution is the only trajectory drifting off to minus infinity.

Since the rational solution (2.12) does not have any free parameter left, as specified in (2.11), there is no possibility to break the \mathcal{PT} -symmetry spontaneously for this type of solution. We may, however, break the \mathcal{PT} -symmetry completely directly on the level of the Hamiltonian by fully complexifying β or γ , an example of which is depicted in figure 1b. As expected we observe that the symmetry $u^*(\zeta) = u(-\zeta)$ has been lost, but instead the trajectories are almost symmetric about the line passing the two points A and $u(0)$, which are now both located away from the real axis. However, the nature of the fixed point, being either an unstable or stable improper node, has not changed.

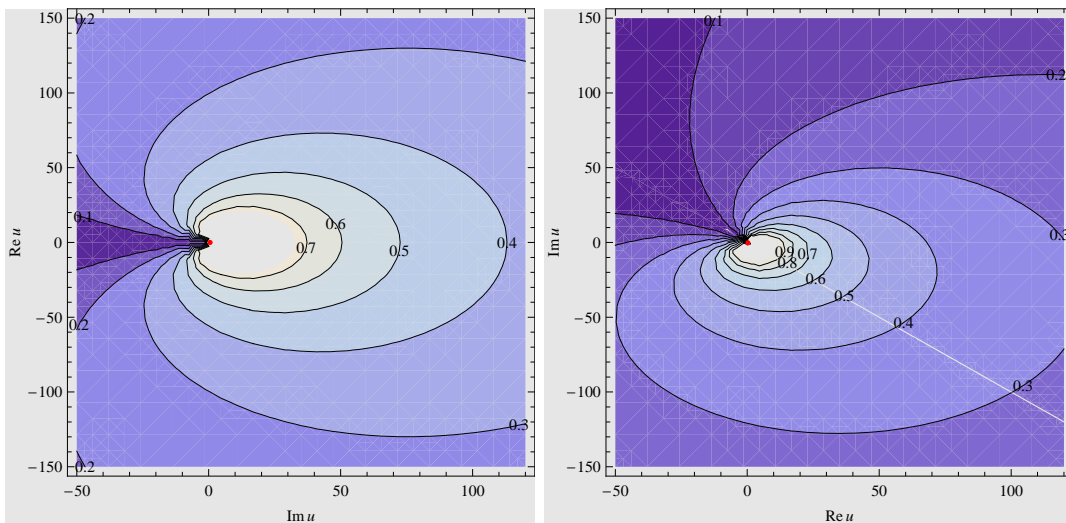


Figure 1: Complex rational solutions of the KdV equation for different values of purely complex initial conditions ζ_0 : (a) \mathcal{PT} -symmetric solutions for $c = 1$, $\beta = 2$, $\gamma = 3$ and $A = 1/2$; (b) Broken \mathcal{PT} -symmetric solutions for $c = 1$, $\beta = 2 + i2$, $\gamma = 3$ and $A = (1 - i)/4$. Different trajectories are characterized by different initial conditions ζ_0 . Some values for the imaginary part of $\text{Im}\zeta_0 < 1$ are indicated on the trajectories. The unresolved white region corresponds to values for $\text{Im}\zeta_0 > 1$. Throughout this manuscript we label panels from the left to the right as (a), (b), (c), etc.

Considering the expression for the energy (1.2) it is evident that it will be real when we have the symmetry $u^*(x) = u(-x)$. We also compute the expression explicitly for the solution (2.12) by substituting it into (1.2). Then the energy in the interval $[-a, a]$ is

computed to

$$E_a = -\frac{ac^2}{3\beta^2} \left(c + \frac{36\gamma}{a^2 - \zeta_0^2} \right) + \frac{72\gamma^2}{15\beta^2} \left[\frac{10c(a^3 + 3a\zeta_0^2)}{(a^2 - \zeta_0^2)^3} - \frac{48\gamma(a^5 + 10a^3\zeta_0^2 + 5a\zeta_0^4)}{(a^2 - \zeta_0^2)^5} \right]. \quad (2.13)$$

Evidently E_a is real even when $i\zeta_0, \beta, \gamma \in \mathbb{R}$ or $i\zeta_0, i\beta, \gamma \in \mathbb{R}$ and complex otherwise, that is for the \mathcal{PT} -symmetric and broken \mathcal{PT} -symmetric case, respectively.

2.1.2 Trigonometric/hyperbolic solutions

As the next possibility for the factorization we specify $P(u) = (u - A)^2(u - B)$ involving now two constants A and B , thus leaving one of them at our disposal when solving (2.5)

$$\lambda = -\frac{\beta}{3\gamma}, \quad \kappa_1 = \frac{A}{2}(\beta A - 2c), \quad \kappa_2 = \frac{A^2}{6}(3c - 2\beta A) \quad \text{and} \quad B = \frac{3c}{\beta} - 2A. \quad (2.14)$$

Having now some freedom in the choice of the constants one may ask which ones are the most natural to use for the symmetry breaking. As we will see the constants A and B have a direct physical meaning and it appears therefore natural to view them as the free parameters to tune for a concrete model with fixed coupling constants β, γ , rather than the integration constants κ_1 or κ_2 emerging more indirectly without immediate interpretation. By (2.7) vanishing asymptotic boundary conditions require the choice $A = 0$.

In general, the solution to (2.6) produces in this case the trigonometric/hyperbolic solution

$$u(\zeta) = B + (A - B) \tanh^2 \left[\frac{1}{2} \sqrt{A - B} \sqrt{\lambda} (\zeta - \zeta_0) \right]. \quad (2.15)$$

Let us first discuss the \mathcal{PT} -symmetric scenario for which all constants are taken to be real except for ζ_0 , which we still allow to be complex. When in that case either $A < B$, $\lambda > 0$ or $A > B$, $\lambda < 0$ we obtain a periodic solution with period $T = 2\pi/(\sqrt{|A - B|}\sqrt{|\lambda|})$ as depicted in figure 2a. The closed trajectories surround the point A , whereas the point B is situated on its outside, following from the fact that on the real axis we always have $u(\zeta) < B$ or $u(\zeta) > B$, in the respective cases. This behaviour is also confirmed by the linearisation (2.9) at the fixed point A . Parameterizing $A - B = r_{AB}e^{i\theta_{AB}}$ and $\lambda = r_\lambda e^{i\theta_\lambda}$ the Jacobian (2.10) is easily computed to

$$J(u)|_{u=A} = \begin{pmatrix} \pm\sqrt{r_{AB}r_\lambda} \cos \left[\frac{1}{2}(\theta_{AB} + \theta_\lambda) \right] \mp\sqrt{r_{AB}r_\lambda} \sin \left[\frac{1}{2}(\theta_{AB} + \theta_\lambda) \right] \\ \pm\sqrt{r_{AB}r_\lambda} \sin \left[\frac{1}{2}(\theta_{AB} + \theta_\lambda) \right] \pm\sqrt{r_{AB}r_\lambda} \cos \left[\frac{1}{2}(\theta_{AB} + \theta_\lambda) \right] \end{pmatrix}, \quad (2.16)$$

with eigenvalues

$$j_1 = \pm\sqrt{r_{AB}r_\lambda} \exp \left[\frac{i}{2}(\theta_{AB} + \theta_\lambda) \right] \quad \text{and} \quad j_2 = \pm\sqrt{r_{AB}r_\lambda} \exp \left[-\frac{i}{2}(\theta_{AB} + \theta_\lambda) \right]. \quad (2.17)$$

Clearly for the two cases here, that is $A < B$, $\lambda > 0$ or $A > B$, $\lambda < 0$, the eigenvalues of the Jacobian are purely complex, i.e. $j_{1/2} = \pm i\sqrt{|A - B|}\sqrt{|\lambda|}$, indicating that the point A is a centre. The result is independent of the sign in (2.8). The linearisation at the fixed point B does not exist, due to the occurrence of the square root.

For this periodic case we may also compute the energy E_T for one period T from $-\pi/\sqrt{|A-B|}\sqrt{|\lambda|}$ to $\pi/\sqrt{|A-B|}\sqrt{|\lambda|}$ analytically to

$$E_T = \oint_{\Gamma} \mathcal{H}[u(\zeta)] \frac{du}{u\zeta} = \oint_{\Gamma} \frac{\mathcal{H}[u]}{\sqrt{\lambda}\sqrt{u-B}(u-A)} du = -\pi\sqrt{\frac{\beta\gamma}{3}} \frac{A^3}{\sqrt{A-B}}. \quad (2.18)$$

Here the contour Γ is taken to be any complex trajectory resulting for $i\zeta_0 \in \mathbb{R}$. Then (2.18) follows from Cauchy's residue theorem and the fact that B will always be outside the contour Γ . We find that the energy is real and takes the same value for all trajectories independently of the concrete choice for the initial condition ζ_0 . Notice that the energy for the real solution, i.e. $\zeta_0 \in \mathbb{R}$, can not be computed in such an easy way as in that case Γ does not form a closed contour. Thus demanding \mathcal{PT} -symmetry leads inevitably to purely complex initial value conditions and constitutes a natural " ϵ -prescription" to deform the real solution with the purpose to compute the energy for one period.

For the remaining possibilities $A > B$, $\lambda > 0$ or $A < B$, $\lambda < 0$ all solutions tend asymptotically to A , which we depict for some examples in figure 2b. The linearisation (2.9) at the fixed point A yields in these cases the two degenerate real eigenvalues $j_1 = j_2 = \sqrt{|A-B|}\sqrt{|\lambda|}$ or $j_1 = j_2 = -\sqrt{|A-B|}\sqrt{|\lambda|}$ for J depending on the plus or minus sign in (2.8), respectively. The Jacobian (2.16) is diagonalisable in these cases and therefore A is an unstable or stable star node. As for the rational solutions, this implies that only the choice with different branches for the upper and lower half will give rise to closed orbits as seen in figure 2b. Now the energies can not be computed in a simple manner as for the periodic case since the singularity at A is situated on the contour.

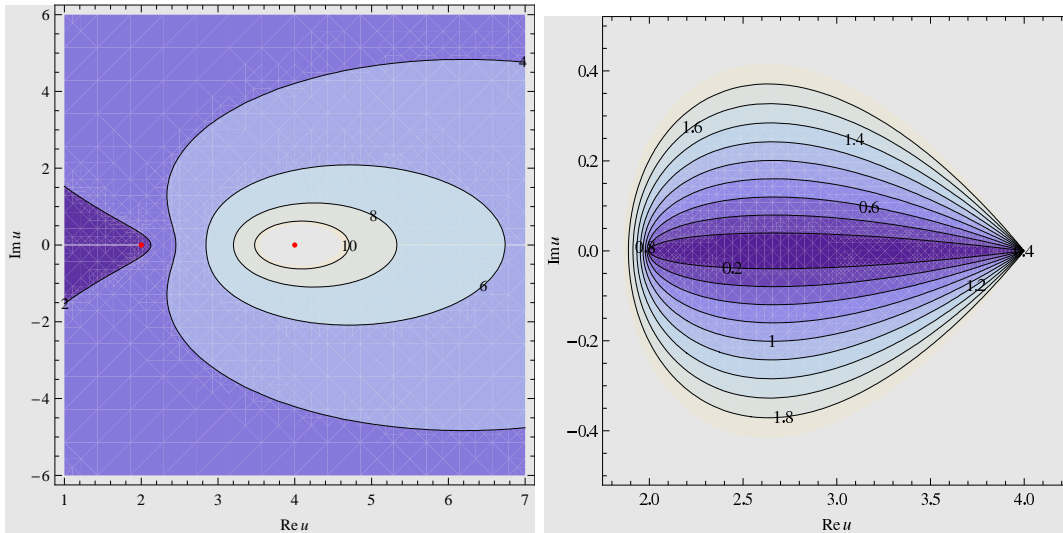


Figure 2: Complex trigonometric/hyperbolic solutions of the KdV equation: (a) \mathcal{PT} -symmetric periodic solutions with $c = 1$, $\beta = 3/10$, $\gamma = 3$, $A = 4$, $B = 2$ and $T = 2\sqrt{15}\pi$; (b) \mathcal{PT} -symmetric asymptotically constant solutions with $c = 1$, $\beta = 3/10$, $\gamma = -3$, $A = 4$ and $B = 2$.

Let us next embark on the case in which the \mathcal{PT} -symmetry is spontaneously broken, which unlike as for the rational solutions, is possible for (2.15) since we have additional

parameters at our disposal. From (2.14) and (2.15) it is clear that when $2\beta\kappa_1 + c^2 < 0$ the constant A becomes complex and we no longer have the property $u^*(\zeta) = u(-\zeta)$ ensuring the reality of the spectrum. The nature of the fixed point is now changed again to an unstable or stable focus depending on whether $\text{Re } j_i > 0$ or $\text{Re } j_i < 0$, respectively. Thus once again closed orbits are obtained with the choice of different branches for the upper and lower half plane. This means of course that the periodic solution ceases to be periodic.

The energies E_T for one period in the periodic solution corresponding to the two choices A, B, ζ_0 and A^*, B^*, ζ_0^* occur in complex conjugate pairs. This is the typical scenario for spontaneously broken \mathcal{PT} -symmetry, i.e. the Hamiltonian is still \mathcal{PT} -symmetric but the solutions to the Schrödinger equation in the quantum case and in the classical case to the equation of motion, are not. Formula (2.18) may still be used in this case for the computation of the energy even though the singularities are moved away from the real axis as they still lie within the contour. Once again the result does not depend on the choice of ζ_0 . We depict some trajectories for this type of spontaneous symmetry breaking in figure 3. The conjugate solution is simply obtained by a reflection about the real axis, as shown explicitly for the asymptotically constant solution in panel (b).

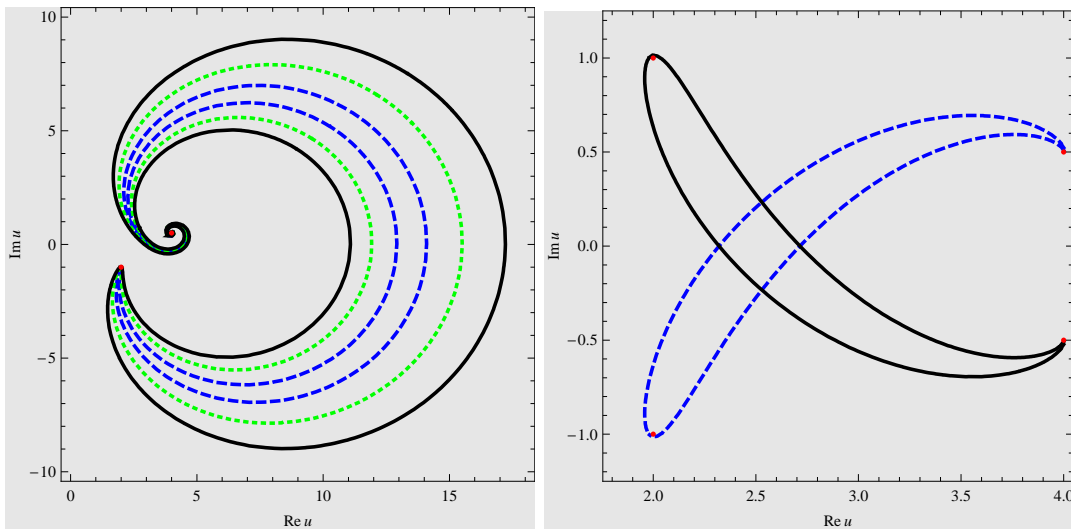


Figure 3: Complex trigonometric/hyperbolic solutions of the KdV equation: (a) Spontaneously broken \mathcal{PT} -symmetry of the periodic solution with $c = 1$, $\beta = 3/10$, $\gamma = 3$, $A = 4 + i/2$ and $B = 2 - i$ for $\text{Im } \zeta_0 = 0.5$ solid (black), $\text{Im } \zeta_0 = 0.3$ dotted (green) $\text{Im } \zeta_0 = 0.1$ dashed (blue); (b) Spontaneously broken \mathcal{PT} -symmetry of the asymptotically constant solution with $c = 1$, $\beta = 3/10$, $\gamma = -3$ for $A = 4 - i/2$, $B = 2 + i$ $\text{Im } \zeta_0 = -0.5$ solid (black) and $A = 4 + i/2$, $B = 2 - i$, $\text{Im } \zeta_0 = 0.5$ dashed (blue).

Finally, there is of course also the possibility to break \mathcal{PT} -symmetry directly for the Hamiltonian itself. For instance when $\beta \notin \mathbb{R}$ and/or $\gamma \notin \mathbb{R}$ we expect the energies to be complex. In that case the complex conjugate energy would be obtained by considering a new type of Hamiltonian with β^* , γ^* and thus it does not arise from within one specific model. We depict an example trajectory for this scenario in figure 4.

We observe from figure 4a that the periodic broken solution near the fixed point is

qualitatively the same as the one for the spontaneously broken case, namely a stable or unstable focus. This behaviour follows from the eigenvalues (2.17), which indicate that there is no distinction at this point in whether the complexification of the j_i result from a spontaneous or a complete breaking of the \mathcal{PT} -symmetry. Note that the trajectories still close even though this is not shown in figure 4a, but this may be seen on a larger scaled plot. We find a similar behaviour for the fixed point of the broken asymptotic solution as depicted in figure 4b.

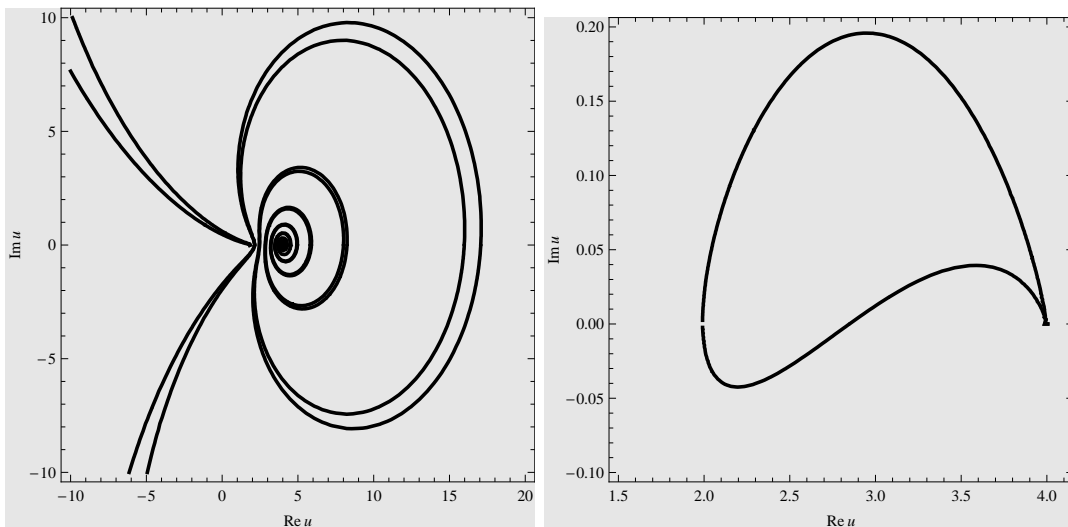


Figure 4: Complex trigonometric/hyperbolic solutions of the KdV equation: (a) Broken \mathcal{PT} -symmetry of the periodic solution with $A = 4$, $B = 2$, $c = 1$, $\beta = 3/10$, $\gamma = 3 + i/2$ and $\text{Im } \zeta_0 = 6$; (b) Broken \mathcal{PT} -symmetry of the asymptotically constant solution with $A = 4$, $B = 2$, $c = 1$, $\beta = 3/10$, $\gamma = 3 + i/2$ and $\text{Im } \zeta_0 = 1/2$.

So far we have simply broken the symmetry by choosing some more or less random complex value for γ . However, we can also carry out this process in a more controlled fashion producing periodic motion and even some non-Hermitian non- \mathcal{PT} -symmetry cases with real energies. First of all we observe from eigenvalues of the Jacobian (2.10) that the fixed point A becomes a centre when $\theta_{AB} + \theta_\lambda = \pi$, which is also compatible with the solution (2.15) from which we notice that a periodic motion occurs when $\lambda(A - B) < 0$. This allows for complex values of the parameters β, γ, A and B . Combining this constraint with the last equation in (2.14) leads to

$$A = \frac{\sin \theta_\gamma}{|\beta| \sin(\theta_\gamma - \theta_\beta - \theta_A)} \exp(i\theta_A). \quad (2.19)$$

Thus, for a given model, that is for *any* fixed values of β and γ we obtain a periodic motion around the point A , given by the expression in (2.19) for any value of θ_A . Indeed this is the case as we observe for instance in figure 5a. When using the constraint $\theta_{AB} + \theta_\lambda = \pi$ for the periodic motion in the expression for the energy (2.18) we find

$$E_T = -\frac{\pi}{3} \frac{\beta A^3}{\sqrt{|\lambda| |A - B|}}. \quad (2.20)$$

Hence, demanding that the energy is to be real leads to the further constraint $3\theta_A + \theta_\beta = 0, \pi$. Implementing this in (2.19) yields

$$E_T \in \mathbb{R} \quad \text{for } A = \frac{\sin \theta_\gamma}{|\beta| \sin(\theta_\gamma - 2\theta_\beta/3)} \exp\left(-i\frac{\theta_\beta}{3}\right). \quad (2.21)$$

This means for a given model, that is for *any* fixed values of β and γ we can find a point A , given by the expression in (2.21), around which the trajectory is periodic and the corresponding energy is real. This holds irrespective of whether β and γ are real or complex, or in other words whether the \mathcal{PT} -symmetry is intact or completely broken. In figure 5b we depict an example solution of (2.21) corresponding to a periodic motion with completely broken \mathcal{PT} -symmetry but real energy. An obvious question to ask at this point is whether by breaking this symmetry the system has acquired a new kind of anti-linear symmetry, which could serve to explain the reality of the energy. A systematic study of this more general issue will be presented elsewhere.

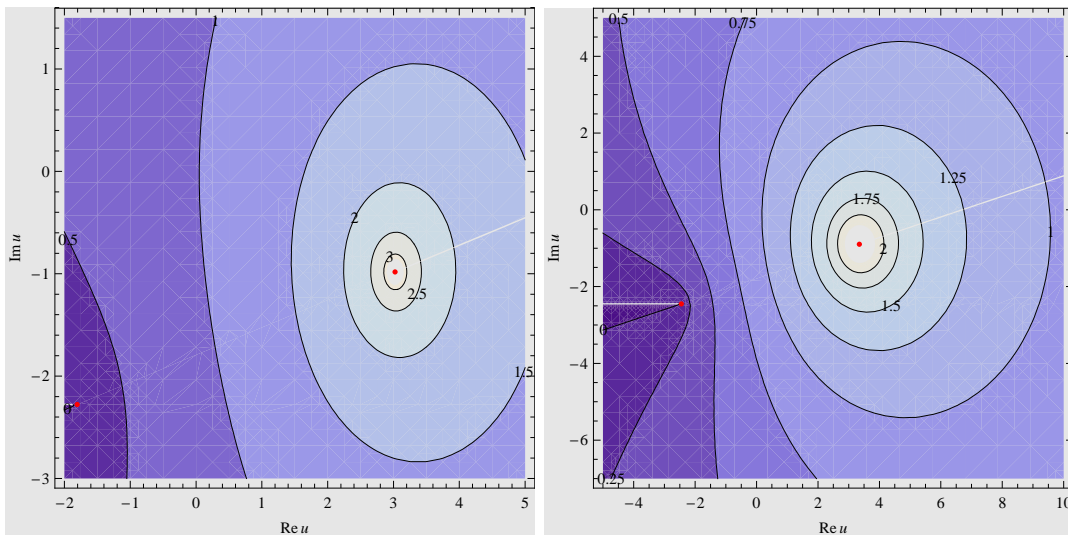


Figure 5: Complex trigonometric/hyperbolic solutions of the KdV equation with completely broken \mathcal{PT} -symmetry: (a) Periodic solution with complex energy $E_T = -10.518 + i1.666$ for $c = 1$, $\beta = 1/2 \exp(i\pi/4)$, $\gamma = 1/3 \exp(i\pi/3)$, $A = \sqrt{3} \sin(11\pi/60) \exp(-i\pi/10) \approx 3.025 - i0.983$ and $B = 6 \exp(-i\pi/4) - 2\sqrt{3} \sin(11\pi/60) \exp(-i\pi/10) \approx -1.806 - i2.277$; (b) Periodic solution with real energy $E_T = -4\pi$ for $c = 1$, $\beta = 1/2 \exp(i\pi/4)$, $\gamma = 1/3 \exp(i\pi/3)$, $A = 2\sqrt{3} \exp(-i\pi/12) \approx 3.346 - i0.896$ and $B = -\sqrt{6}(1 + i) \approx -2.449 - i2.449$.

In general we observe from the various cases studied in this subsection that when we let the parameters vary one of the fixed points for the periodic solution undergoes a Hopf bifurcation, i.e. it changes its behaviour from a stable focus to a centre and then to an unstable focus. As we can see from (2.17) this behaviour is governed by the sign of $\pm \cos\left[\frac{1}{2}(\theta_{AB} + \theta_\lambda)\right]$ this bifurcation can be achieved either by a spontaneous symmetry breaking, that is by varying the free parameter A , or by a complete breaking of the symmetry, by varying β or γ . Both cases pass through the \mathcal{PT} -symmetric case as realised by the centre.

2.1.3 Elliptic solutions

Next we specify $P(u) = (u - A)(u - B)(u - C)$ with three constants A , B and C leaving two constants at our disposal when solving (2.5)

$$\lambda = -\frac{\beta}{3\gamma}, \quad \kappa_1 = \frac{1}{6} [\beta(A^2 + AC + C^2) - 3c(A - C)], \quad (2.22)$$

$$\kappa_2 = \frac{AC}{6} [3c - \beta(A + C)] \quad \text{and} \quad B = \frac{3c}{\beta} - (A + C). \quad (2.23)$$

Vanishing asymptotic boundary conditions reduce this case to the previous one as by (2.7) they require either $A = B = 0$, $A = C = 0$ or $B = C = 0$. The evaluation of (2.6) yields in this case the elliptic solution

$$u(\zeta) = A + (B - A) \text{ns}^2 \left[\frac{1}{2} \sqrt{B - A} \sqrt{\lambda} (\zeta - \zeta_0) \left| \frac{A - C}{A - B} \right. \right], \quad (2.24)$$

with $\text{ns}(z|m)$ being one of the Jacobi elliptic functions. Therefore $u(\zeta)$ is a double periodic function

$$u(\zeta) = u(\zeta + \omega_1 + \omega_2) \quad (2.25)$$

with periods

$$\omega_1 = \frac{8}{\sqrt{B - A} \sqrt{\lambda}} K \left(\frac{A - C}{A - B} \right) \quad \text{and} \quad \omega_2 = i \frac{16}{\sqrt{B - A} \sqrt{\lambda}} K \left(\frac{C - B}{A - B} \right). \quad (2.26)$$

Here $K(m)$ denotes a complete elliptic integral of the first kind. As expected we recover the previous case when two of the constants A, B, C coincide as in these cases the periods become dependent on each other, i.e. $\lim_{A \rightarrow B} \omega_1/\omega_2 = 1/2 \text{sign}(C - A)$, $\lim_{A \rightarrow C} \omega_1/\omega_2 = -i\infty$ and $\lim_{B \rightarrow C} \omega_1/\omega_2 = 0$.

Studying at first the \mathcal{PT} -symmetric solutions, we find periodic solutions encircling some of the fixed points. For instance in figure 6 we depict an example in which the fixed points A and B are encircled, whereas C is situated outside of the trajectories. Different types of scenarios are also expected, changing for instance the sign in γ will lead to a periodic orbit surrounding the points B and C .

Next we break the \mathcal{PT} -symmetry spontaneously by complexifying the free parameters of the solutions. We find that the periodic trajectories open up and cease to be periodic. In figure 7a we trace part of the trajectory to illustrate the behaviour. Starting at the point $u(-64) \approx 7.19 + i0.74$ the trajectory passes down between the points A and B and moves then up again surrounding once the points C and A in a clockwise sense. Thereafter it encircles C once more but instead of moving around A it passes inbetween C and A surrounding A in an anti-clockwise sense. It keeps progressing in an anti-clockwise manner encircling C before passing from below between the points A and B reaching the point $u(18) \approx 6.36 + i3.45$. It appears that this type of movement is repeated indefinitely. In figure 7b we depict a wider range for ζ indicating that the region of the phase space depicted will eventually be filled densely by the trajectory, hence suggesting a chaotic behaviour. However, we do not observe a sensitivity towards the initial condition, which would be typical for a proper chaotic system.

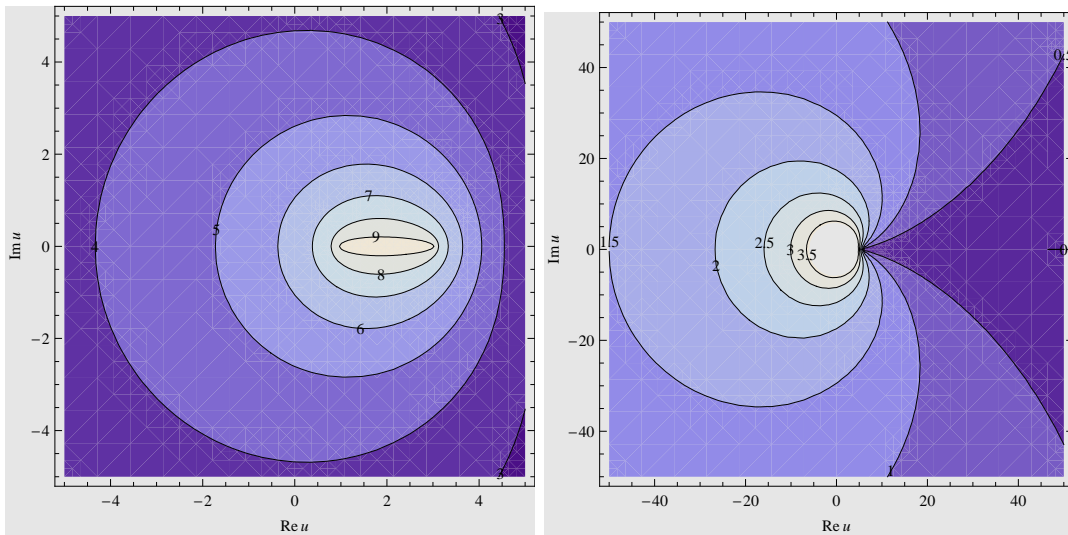


Figure 6: \mathcal{PT} -symmetric complex elliptic solutions of the KdV equation with $A = 1$, $B = 3$, $C = 6$, $c = 1$, $\beta = 3/10$, $\gamma = -3$ for different values of $\text{Im } \zeta_0$.

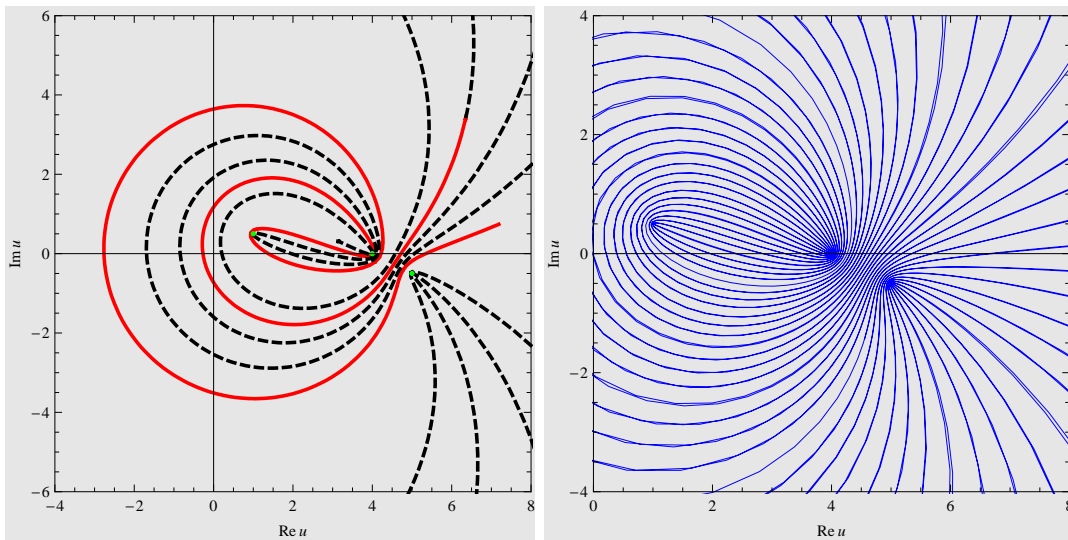


Figure 7: Spontaneously broken \mathcal{PT} -symmetric complex elliptic solutions of the KdV equation for $\text{Im } \zeta_0 = 6$ with $A = 4$, $B = 5 - i/2$, $C = 1 + i/2$, $c = 1$, $\beta = 3/10$ and $\gamma = 3$: (a) $-64 \leq \zeta \leq 18$ solid (red) and $18 < \zeta \leq 200$ dashed (black); (b) $-200 < \zeta < 1400$.

Finally we may also break the \mathcal{PT} -symmetry completely by complexifying the parameters of the model β or/and γ . Examples for such a scenario are depicted in figure 8. The behaviour is similar to the one of the spontaneously broken case, i.e. the periodic motion has turned into open trajectories with a noncompact limit set. Increasing the range for ζ will fill the depicted part of the phase space similarly as in the spontaneously broken \mathcal{PT} -symmetry case, thus suggesting a chaotic behaviour, albeit once again we do not observe the typical sensitivity towards the initial conditions.

Figures 7 and 8 are very reminiscent of the plots which may be found in section 5 of

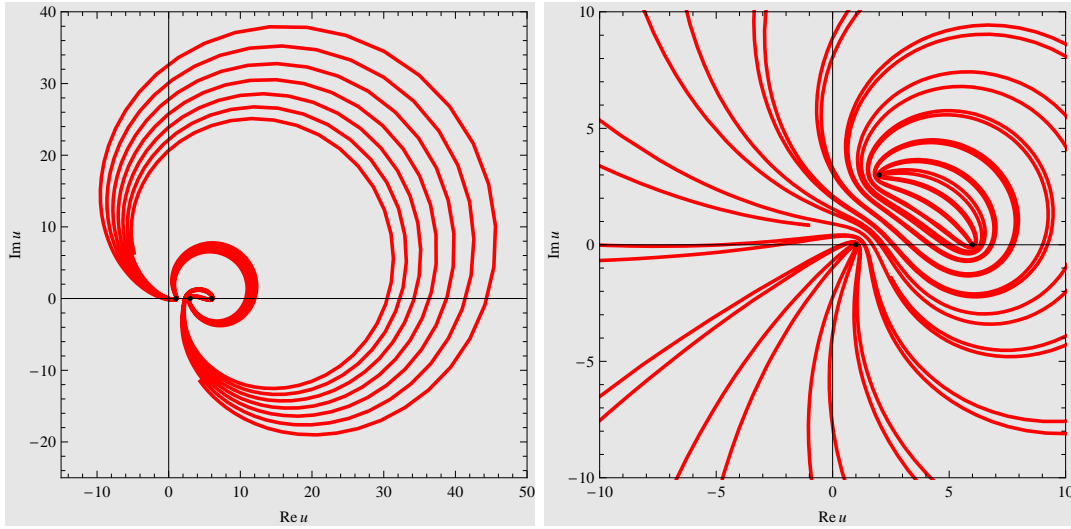


Figure 8: Broken \mathcal{PT} -symmetric complex elliptic solutions of the KdV equation for $\text{Im } \zeta_0 = 6$: (a) $A = 1$, $B = 3$, $C = 6$, $c = 1$, $\beta = 3/10$ and $\gamma = 3 + 2i$ for $-200 \leq \zeta \leq 200$; (b) $A = 1$, $B = 2 + 3i$, $C = 6$, $c = 1$, $\beta = 3/10 - i/10$ and $\gamma = 3$ for $-200 \leq \zeta \leq 200$.

reference [12]. This is not surprising as formally the differential equations solved in there for the quantum mechanical setting for the potential $V \sim x^3$ are special cases of our more general treatment when making the identification $u \rightarrow x$ and $\zeta \rightarrow t$ for our traveling wave equation. With the further identifications

$$\kappa_1 = 0, \quad \kappa_2 = \gamma E, \quad \beta = 6cg \quad \text{and} \quad \gamma = -c \quad (2.27)$$

equation (2.5) converts precisely into the quantum mechanical Hamiltonian

$$H = E = \frac{1}{2}p^2 + \frac{1}{2}x^2 - gx^3, \quad (2.28)$$

treated in [12]. The identification (2.27) explains why no analogue to our rational solution was found in [12], since $\kappa_1 = 0$ implies $c = 0$ and therefore the vanishing of κ_2 , i.e. the confining potential, and A . However, as can be seen from (2.14) there should be an analogue to our trigonometric solution with energy $E = -4c^3/\gamma\beta^2$ when setting $A = 2c/\beta$. This energy depends on the coupling constant and is of course not freely choosable as in the elliptic case presented in this section where κ_2 is a free parameter. More potentials of the type treated in [12] can be obtained systematically from the deformations discussed below.

The new elliptic solutions recently found for generalized shallow wave equations [37] are expected to exhibit a similar behaviour as the solution discussed in this subsection.

2.1.4 Soliton solutions

There exist various techniques to construct soliton solutions. Here we briefly recall and apply Hirota's direct method [38] for that purpose. The starting point of this approach is Hirota's bilinear form, which reads in general

$$p(D)\tau \cdot \tau = 0, \quad (2.29)$$

with $p(D)$ being a polynomial in the Hirota derivatives, i.e. $D_x f \cdot g = f_x \cdot g - f \cdot g_x$ where the dot "·" indicates the noncommutative nature of the product $f \cdot g$. The soliton solutions to (2.29) may then be constructed perturbatively order by order in ε from the expansion

$$\tau = \sum_{n=0}^{\infty} \varepsilon^n \tau_n. \quad (2.30)$$

Defining the function $\tau(x, t)$ via the relation

$$u(x, t) = \frac{12\gamma}{\beta} (\ln \tau)_{xx}, \quad (2.31)$$

the KdV-equation (2.2) can be brought into Hirota's bilinear form

$$\frac{6\gamma}{\beta} (\gamma D_x^4 + D_x D_t) \tau \cdot \tau = 0. \quad (2.32)$$

We have set here the integration constant to zero. Taking the zeroth order solution to be $\tau_0 = 1$ the first order tau-function results to $\tau_1(x, t) = \exp(p_1 x - \gamma p_1^3 t + \phi_1)$ and we obtain the well-known one-soliton solution up to this order

$$u(x, t) = \frac{3\gamma p_1^2}{\beta \cosh^2 \left[\frac{1}{2}(p_1 x - \gamma p_1^3 t + \phi_1) \right]}. \quad (2.33)$$

A \mathcal{PT} -symmetric variant of this solution is depicted in figure 9a. As expected the origin in the u -plane is an asymptotic fixed point, reached for $x \rightarrow \pm\infty$ or $t \rightarrow \pm\infty$.

Breaking the \mathcal{PT} -symmetry in various ways yields more unexpected results. Regarding p_1, ϕ_1, ζ_0 as parameters of the solution and β, γ as model defining constants, their complexification constitutes a spontaneous or complete \mathcal{PT} -symmetry breaking, respectively. The corresponding solutions in the u -plane appear as distorted versions of the symmetric case, as can be seen in figure 9b. An interesting feature of the broken complex solution is that, unlike its real counterpart, the soliton does not maintain its overall shape while traveling. Instead, it becomes a breather and regains its shape after a certain distance Δ_x and certain amount of time Δ_t governed by the equation

$$u(x + \Delta_x, t) = u(x, t + \Delta_t). \quad (2.34)$$

Separating γ, p_1 into their real and imaginary part as $\gamma = \gamma_r + i\gamma_i$ and $p_1 = p_r + ip_i$, we can solve (2.34) for the one-soliton solution (2.33) to

$$\Delta_t = \frac{2\pi p_r}{(p_i^4 - p_r^4) \gamma_i - 2p_i p_r (p_i^2 + p_r^2) \gamma_r}, \quad (2.35)$$

$$\Delta_x = 2\pi \frac{p_i (3p_r^2 - p_i^2) \gamma_i + 2\pi p_r (3p_i^2 - p_r^2) \gamma_r}{(p_i^4 - p_r^4) \gamma_i - 2p_i p_r (p_i^2 + p_r^2) \gamma_r}. \quad (2.36)$$

The speed of the soliton is therefore given by

$$v = -\frac{\Delta_x}{\Delta_t} = (3p_i^2 - p_r^2) \gamma_r - \frac{p_i (p_i^2 - 3p_r^2) \gamma_i}{p_r}. \quad (2.37)$$

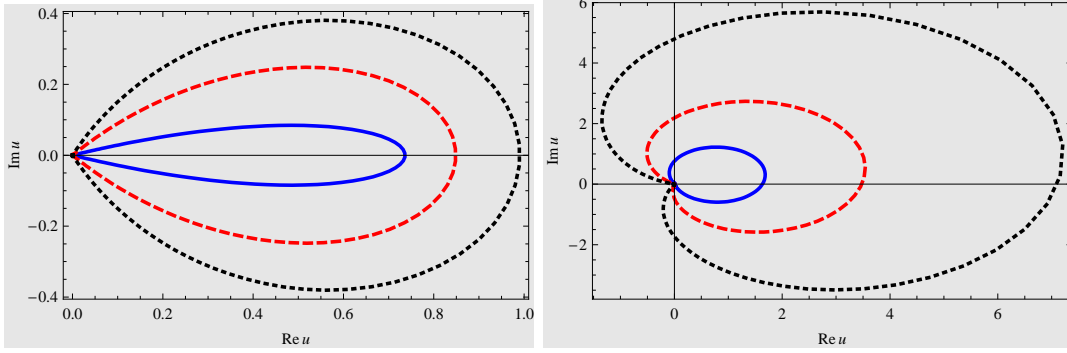


Figure 9: Complex one-soliton solution of the KdV-equation at fixed time $t = -2$: (a) \mathcal{PT} -symmetric solution with $\beta = 6$, $\gamma = 1$, $p_1 = 1.2$ for $\phi = i0.3$ solid (blue), $\phi = i0.8$ dashed (red) and $\phi = i1.1$ dotted (black); (b) Broken \mathcal{PT} -symmetric solution with $\beta = 6$, $\gamma = 1 + i0.4$, $p_1 = 1.2$ for $\phi = i0.3$ solid (blue), $\phi = i0.8$ dashed (red) and $\phi = i1.1$ dotted (black).

Clearly for the \mathcal{PT} -symmetric solution the shape will be the same in the u -plane even at different times, whereas the complex solution will change its shape as we observe in figure 9. In figure 10 we observe that the one-soliton changes its shape while progressing in time but regains it after $\Delta_t = -\pi/2$ for the chosen values.

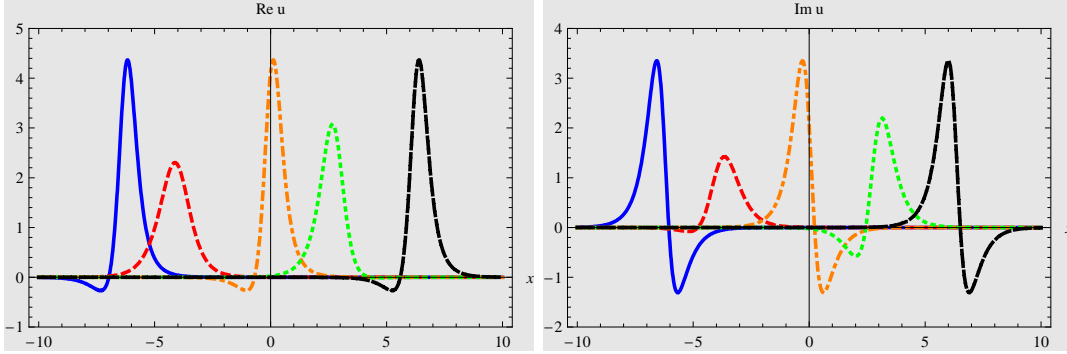


Figure 10: Complex spontaneously broken one-soliton solution of the KdV-equation with $\beta = 6$, $\gamma = 1 + i/2$, $p_1 = 2$, $\phi = i0.8$ and $\Delta_t = -\pi/2$ for different times $t = -\pi/2$ solid (blue), $t = -1$ dashed (red), $t = 0$ dasheddot (orange), $t = 0.7$ dotted (green), and $t = \pi/2$ dasheddotdot (black) (a) real part; (b) imaginary part.

Proceeding to the next order in ϵ we compute the two soliton solution to

$$u(x, t) = \frac{24\gamma \sum_{k=0}^6 c_k (-1)^k p_2^k p_1^{6-k}}{\beta (p_1 + p_2)^4 \left[2 \cosh\left(\frac{1}{2}(\eta_1 - \eta_2)\right) + e^{-\frac{\eta_1}{2} - \frac{\eta_2}{2}} \left(\frac{e^{\eta_1 + \eta_2} (p_1 - p_2)^4}{(p_1 + p_2)^4} + 1 \right) \right]^2} \quad (2.38)$$

where we abbreviated $\eta_i = p_i x - \gamma p_i^3 t + \phi_i$ for $i = 1, 2$ with

$$c_0 = 1 + \cosh \eta_2, \quad c_1 = 4 \sinh \eta_2, \quad c_2 = \cosh \eta_1 + 6 \cosh \eta_2 - 1, \quad c_3 = 4(\sinh \eta_1 + \sinh \eta_2) \quad (2.39)$$

and used the symmetry relations $c_i(\eta_1, \eta_2) = c_{6-i}(\eta_2, \eta_1)$. We depict the time evolution of this solution in figures 11 and 12.

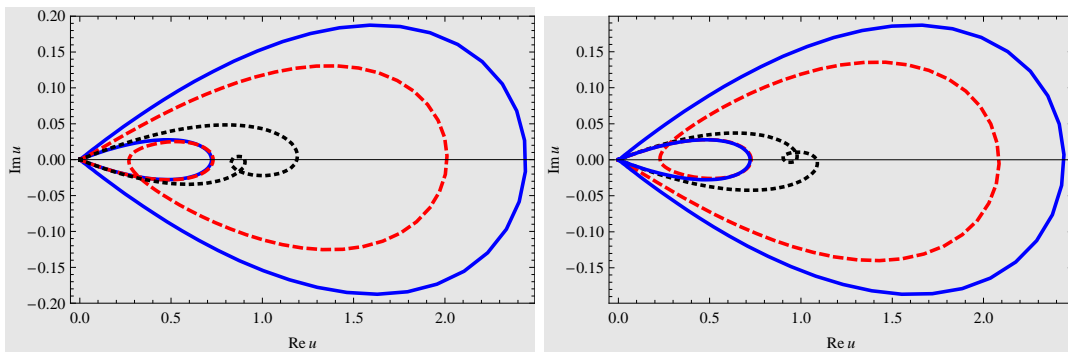


Figure 11: \mathcal{PT} -symmetric two-soliton solutions of the KdV equation for $\beta = 6$, $\gamma = 1$, $p_1 = 1.2$, $p_2 = 2.2$, $\phi_1 = i0.1$ and $\phi_2 = i0.2$. (a) $t = -2$ solid (blue), $t = -0.2$ dashed (red), $t = 0.2$ dotted (black); (b) $t = 0.3$ dotted (black), $t = 0.8$ dashed (red), $t = 2.0$ solid (blue).

We observe in figure 11 the typical scenario for soliton scattering, albeit in the complex plane. For large negative time the two-solitons are separated, indicated here by two individual one-soliton solutions resembling the type depicted in figure 9 touching each other only in the asymptotic point at the origin. In the scattering regime the two solutions merge in a non \mathcal{PT} -symmetric manner until they separate again for large positive time, acquiring once again their individual one-soliton shape.

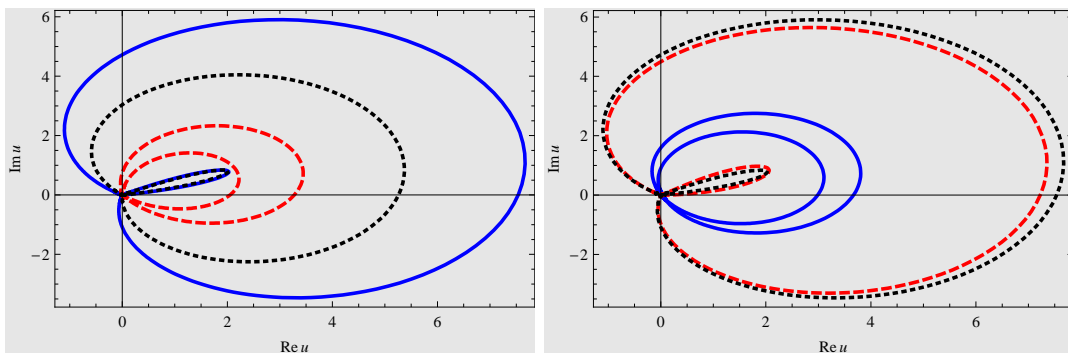


Figure 12: Broken \mathcal{PT} -symmetric two-soliton solutions of the KdV equation for $\beta = 6$, $\gamma = 1 + i\pi/8$, $p_1 = 2(2/3)^{1/3}$, $p_2 = 2$, $\phi_1 = i0.1$ and $\phi_2 = i0.2$. (a) $t = -4$ solid (blue), $t = -3.5$ dashed (red), $t = -2$ dotted (black); (b) $t = 0.7$ solid (blue), $t = 2$ dashed (red), $t = 8$ dotted (black).

For the values in figure 12 the periods for the one-soliton breather to regain its shape with p_1 and p_2 are computed by (2.35) to be $\Delta_t^1 = -3$ and $\Delta_t^2 = -2$, respectively. Indeed we observe in figure 12a that one of the solitons has recovered its shape comparing the solutions at $t = -4$ and $t = -2$. In figure 12b we observed that both solitons have almost regained their original shape passing from $t = 2$ to $t = 8$, that is after $2\Delta_t^1 = 3\Delta_t^2$. The slight discrepancy visible in the figure is due to the well known time delay occurring in a multi-soliton scattering, see e.g. [39].

The energy for the one-soliton solution on the interval $(-\infty, \infty)$ is easily computed

with formula (1.2)

$$E_{1s} = -\frac{36\gamma^3 p_1^5}{5\beta^2}, \quad (2.40)$$

exhibiting the typical behaviour, that is being real for the \mathcal{PT} -symmetric case and complex for the (spontaneously) broken scenario. The integral (1.2) with $u(x, t)$ given by two-soliton solution (2.38) is not easily computed analytically. For large values of time we compute numerically real energies for \mathcal{PT} -symmetric solutions, for instance for the values used in figure 11 we obtain $E_{2s} \approx -10.8049 = E_{1s}(p_1) + E_{1s}(p_2)$. On the other hand we compute complex energies for broken \mathcal{PT} -symmetric solutions, such as for the values used in figure 12 for which we evaluate $E_{2s} \approx -7.8876 - i9.4327 = E_{1s}(p_1) + E_{1s}(p_2)$. This means that in all scenarios the energy of the two-soliton equals the sum of the two separate one-solitons.

3. \mathcal{PT} -symmetric deformations of the KdV equation

Employing the standard arguments used in the study of non-Hermitian Hamiltonian systems with real eigenvalues, we may now \mathcal{PT} -symmetrically deform the Hamiltonian and maintain the possibility to have well defined physical systems, e.g. we still obtain real energies resulting from the new models despite their non-Hermitian nature. The general principle is simply to deform \mathcal{PT} -anti-symmetric quantities, that means if we have the property $\mathcal{PT} : \phi(x, t) \mapsto -\phi(x, t)$ for some field $\phi(x, t)$, we define a deformation map $\delta_\varepsilon : \phi(x, t) \mapsto -i[i\phi(x, t)]^\varepsilon$. The undeformed case is recovered in the limit $\varepsilon = 1$. The new quantity will remain anti- \mathcal{PT} -symmetric with the crucial difference that the overall minus sign is generated from the antilinear nature of the \mathcal{PT} -operator, i.e. $i \mapsto -i$, rather than from $\phi(x, t) \mapsto -\phi(x, t)$. This means for the Hamiltonian resulting from the density (2.1) we can make use of either of the two possibilities

$$\delta_\varepsilon^+ : u_x \mapsto u_{x,\varepsilon} := -i(iu_x)^\varepsilon \quad \text{or} \quad \delta_\varepsilon^- : u \mapsto u_\varepsilon := -i(iu)^\varepsilon, \quad (3.1)$$

depending on whether we choose $u(x, t)$ to be \mathcal{PT} -symmetric or \mathcal{PT} -anti-symmetric, respectively. Accordingly we define the deformed models with some suitable normalisation by the following Hamiltonian densities

$$\mathcal{H}_\varepsilon^+ = -\frac{\beta}{6}u^3 - \frac{\gamma}{1+\varepsilon}(iu_x)^{\varepsilon+1}, \quad \text{and} \quad \mathcal{H}_\varepsilon^- = \frac{\beta}{(1+\varepsilon)(2+\varepsilon)}(iu)^{\varepsilon+2} + \frac{\gamma}{2}u_x^2, \quad (3.2)$$

with corresponding equations of motion

$$u_t + \beta uu_x + \gamma u_{xxx,\varepsilon} = 0 \quad \text{and} \quad u_t + i\beta u_\varepsilon u_x + \gamma u_{xxx} = 0, \quad (3.3)$$

respectively. The Hamiltonian $\mathcal{H}_\varepsilon^+$ was proposed in [24] whereas $\mathcal{H}_\varepsilon^-$ corresponds to a complex version of the generalized KdV equation. For the higher deformed derivatives we use here the notation $u_{xx,\varepsilon} := \partial_x u_{x,\varepsilon}$, $u_{xxx,\varepsilon} := \partial_x^2 u_{x,\varepsilon}, \dots, u_{nx,\varepsilon} := \partial_x^{n-1} u_{x,\varepsilon}$, which means we only deform the first derivative and keep acting on it with ∂_x to define the higher order derivatives. On the level of the equation of motion we could also deform the dispersion term proportional to β , as investigated in [23] for the KdV-equation. However, such deformations do not lead to Hamiltonian systems and the question of how \mathcal{PT} -symmetry may be utilized in this scenario remains an open issue.

Let us now present some solutions to these equations.

3.1 The $\mathcal{H}_\varepsilon^+$ -models

Proceeding similarly as in the previous section, we integrate the first equation in (3.3) twice and obtain the deformed version of equation (2.5)

$$u_\zeta^{(n)} = \exp \left[\frac{i\pi}{2(\varepsilon + 1)}(1 - \varepsilon + 4n) \right] [\lambda_\varepsilon P(u)]^{\frac{1}{1+\varepsilon}}, \quad (3.4)$$

where we abbreviated $\lambda_\varepsilon = -\beta(1 + \varepsilon)/(6\gamma\varepsilon)$ and denote different branches by n . The polynomial $P(u)$ is identical to the one introduced in (2.5), which means we can employ the same factorization as in the previous section. Integrating once more yields

$$\zeta^{(n)} - \zeta_0 = \exp \left[\frac{i\pi}{2(\varepsilon + 1)}(\varepsilon - 1 + 4n) \right] \int du \frac{1}{[\lambda_\varepsilon P(u)]^{\frac{1}{1+\varepsilon}}}. \quad (3.5)$$

We may now proceed as before and specify further the form of $P(u)$. As for the case $\varepsilon = 1$, in some specific cases we succeed to compute the remaining integral and subsequently solve the resulting equation for u , thus obtaining $u(\zeta)$. However, even when this is not possible analytically we can still investigate (3.5) numerically for *all* cases by viewing ζ as a function of the complex variable u and plotting the contours of $\text{Im}[\zeta(u)] = \zeta_0$ in the u -plane, while taking special care about the different Riemann sheets labeled by n . One should distinguish here these type of Riemann sheets from those arising due to the technique employed in our solution procedure. Considering ζ as a function of u , as we do in some intermediate steps, will introduce new branch cuts which are sometimes seen in our figures, e.g. figure 27b. However, we do not attribute any meaning to them in the u -plane. Genuine branch cuts can always be distinguished from the “technical” ones by the fact that they have to be connected to the fixed points which are branch points.

3.1.1 Rational solutions

We start with the same assumption as in the previous section, namely $P(u) = (u - A)^3$, which will impose the same constraints (2.11) for the factorization. The case $\varepsilon = 2$ is special since we may take the root $1/3$ in this case. Integrating (3.5) and solving the result for u we find

$$u^{(n)}(\zeta) = A + \exp \left[-\frac{ie^{-\frac{2}{3}in\pi}}{2^{2/3}} \left(\frac{\beta}{\gamma} \right)^{1/3} (\zeta - \zeta_0) \right]. \quad (3.6)$$

For the remaining integer values $\varepsilon \in \mathbb{Z} \setminus \{2\}$ we can compute also a particular solution

$$u(\zeta) = \frac{c}{\beta} + \exp \left(\frac{i\pi}{2} \frac{5 + \varepsilon}{2 - \varepsilon} \right) \left(\frac{6\gamma\varepsilon}{\beta} \right)^{\varepsilon-2} (1 + \varepsilon)^{\frac{\varepsilon}{\varepsilon-2}} (\varepsilon - 2)^{\frac{\varepsilon+1}{\varepsilon-2}} (\zeta - \zeta_0)^{\frac{\varepsilon+1}{\varepsilon-2}}. \quad (3.7)$$

However, in general we have to take care about the different branches present in (3.5). Our numerical findings for some specific cases are depicted in the figures below.

We supplement our numerical analysis with the prediction of some analytical features. Of special interest are the lines approaching or leaving the fixed points radially. When the symmetry is unbroken they can be defined equivalently as the lines for which $\zeta_0 = 0$. We compute them by noting first that on one hand any point \tilde{u} on the line radially crossing the

point $u = A$ is characterized by a constant value for $\arg(\tilde{u} - A) =: \theta_0$. On the other hand the change of u with respect to ζ has to point into the same direction, i.e. $\arg(\pm\tilde{u}_\zeta) = \theta_0$. Hence the lines of real initial conditions are determined by solving

$$\arg(\pm\tilde{u}_\zeta^{(n)}) = \arg(\tilde{u}^{(n)} - A) + 2\pi m. \quad (3.8)$$

Employing (3.4) and the factorized form of $P(u)$ we can solve (3.8), obtaining

$$\begin{aligned} \theta_0^{(n,m,\pm)} & : = \arg(\tilde{u}^{(n)} - A) \\ & = \frac{\pi}{2(2-\varepsilon)} [\varepsilon - 1 + 4(m - n + m\varepsilon) - (1 + \varepsilon)(1 \pm 1)] + \frac{1}{\varepsilon - 2} \arg \lambda_\varepsilon \end{aligned} \quad (3.9)$$

for the angle in which the trajectories with $\zeta_0 = 0$ enter the point A .

In figure 13 we show the first two members of the sequel parameterizing the deformation parameter as $\varepsilon = -n/(n+1)$ with $n = 1, 2, \dots$. We observe that the pictures resemble flowers with $4 + 6n$ petals. We may predict the number of petals analytically as they are equal to the number of $\zeta_0 = 0$ solutions computable by (3.9). For instance for the case $n = 3$ the formula (3.9) predicts the 16 values $\theta_0 = (2\ell - 1)\pi/16$ for the parameter choice $c = 1$, $\beta = 2$ and $\gamma = 3$ with $\ell = 1, \dots, 16$. We recognize these values in figure 13b. Note that the wedge regions separate different solutions from each other as the point A is always an asymptotic fixed point.

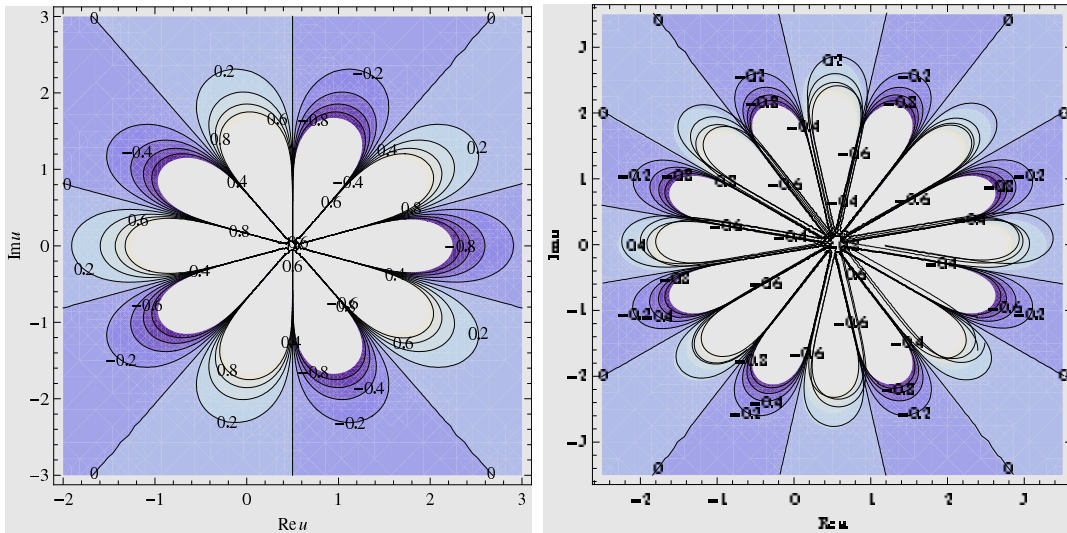


Figure 13: Complex \mathcal{PT} -symmetric rational solutions of the deformed KdV equation with $A = 1/2, c = 1, \beta = 2$ and $\gamma = 3$ for (a) $\mathcal{H}_{-1/2}^+$ and (b) $\mathcal{H}_{-2/3}^+$.

The trajectories appear to be qualitatively quite different for negative integer values of ε . For instance in figure 14a and 14b we depict some trajectories for the models with $\varepsilon = -2$ and $\varepsilon = -3$, respectively. It appears that the fixed point A is more like a saddle point, i.e. we exhibit trajectories more of a hyperbolic nature running away to infinity rather than converging asymptotically to A as in figure 13. The $\zeta_0 = 0$ solutions are predicted once again correctly by (3.9) to be at $\theta_0 = (2\ell - 1)\pi/8$ and $\theta_0 = (2\ell - 1)\pi/5$.

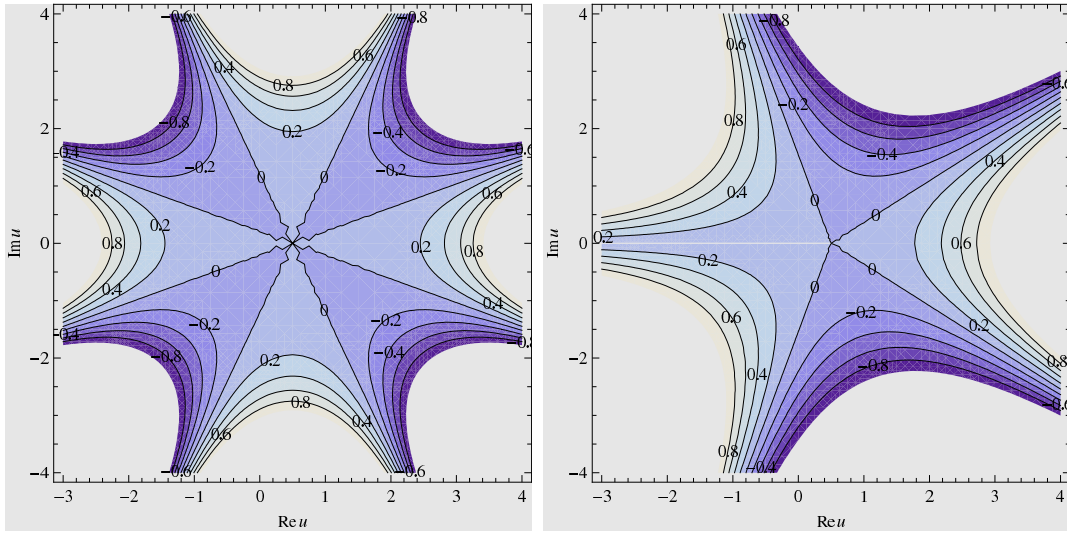


Figure 14: Complex \mathcal{PT} -symmetric rational solutions of the deformed KdV equation with $A = 1/2$, $c = 1$, $\beta = 2$ and $\gamma = 3$ for (a) \mathcal{H}_{-2}^+ and (b) \mathcal{H}_{-3}^+ .

For positive rational values of ε a complete trajectory extends over several different Riemann sheets. Figure 15a and 15b show the solutions $\zeta^{(1)}$ and $\zeta^{(2)}$, respectively. The angles for the $\zeta_0 = 0$ solutions are predicted correctly by (3.9) to be $\theta_0 = 4\ell\pi/5$ for $\ell = 1, \dots, 5$. A closed trajectory is obtained when passing the branch cut at $-\infty$ to $1/2$ from the upper half plane in panel (a) to the lower half plane in panel (b). In figure 17a a single trajectory is depicted for $\text{Im } \zeta_0 = 1$.

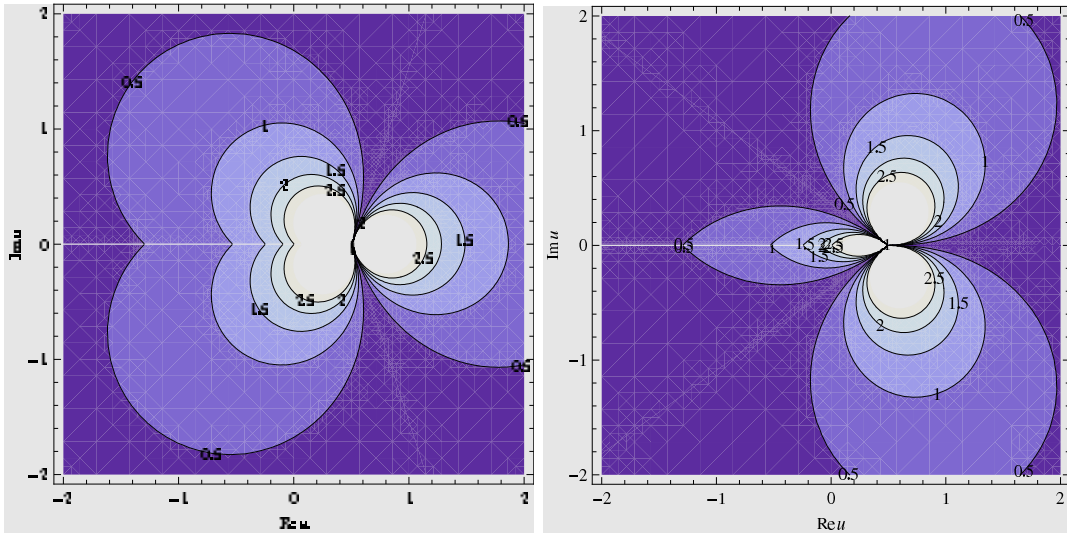


Figure 15: \mathcal{PT} -symmetric rational solutions for $\mathcal{H}_{1/3}^+$: Different Riemann sheets for $A = 1/2$, $c = 1$, $\beta = 2$ and $\gamma = 3$ (a) $\zeta^{(1)}$ and (b) $\zeta^{(2)}$.

For the broken \mathcal{PT} -symmetry we present the solution in figure 16. The branch cut at $-\infty - i/4$ to $(1 - i)/4$ is passed from above in panel (a) to below in panel (b). This

is illustrated in figure 17b, where we depict just one single trajectory for $\text{Im } \zeta_0 = 1$. The trajectories for the \mathcal{PT} -symmetric and broken \mathcal{PT} -symmetric case look qualitatively very similar, the major difference being that the fixed point has moved away from the real axis, thus leading to a loss of the symmetry.

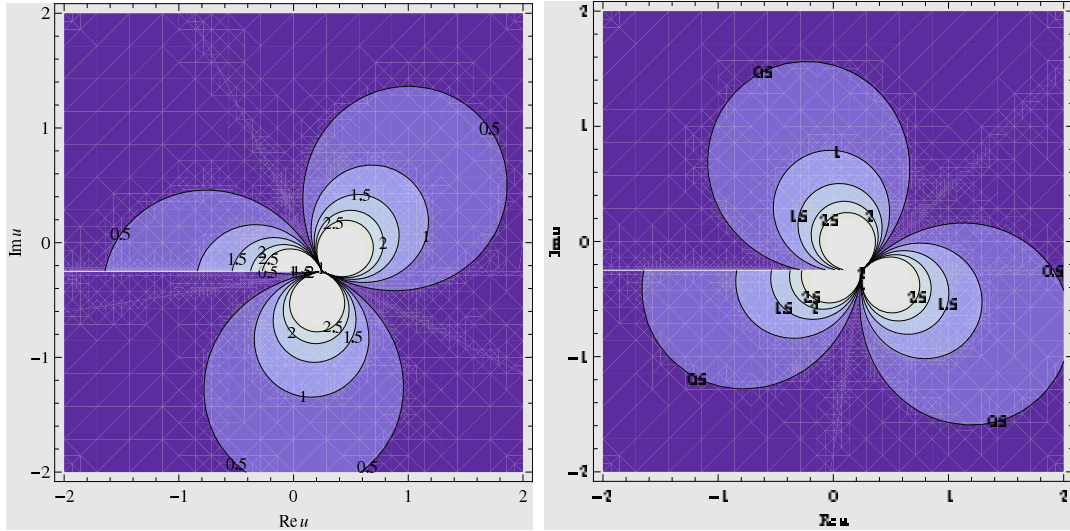


Figure 16: Broken \mathcal{PT} -symmetric rational solutions for $\mathcal{H}_{1/3}^+$: Different Riemann sheets for $A = (1 - i)/4$, $c = 1$, $\beta = 2 + 2i$ and $\gamma = 3$ (a) $\zeta^{(1)}$ and (b) $\zeta^{(2)}$.

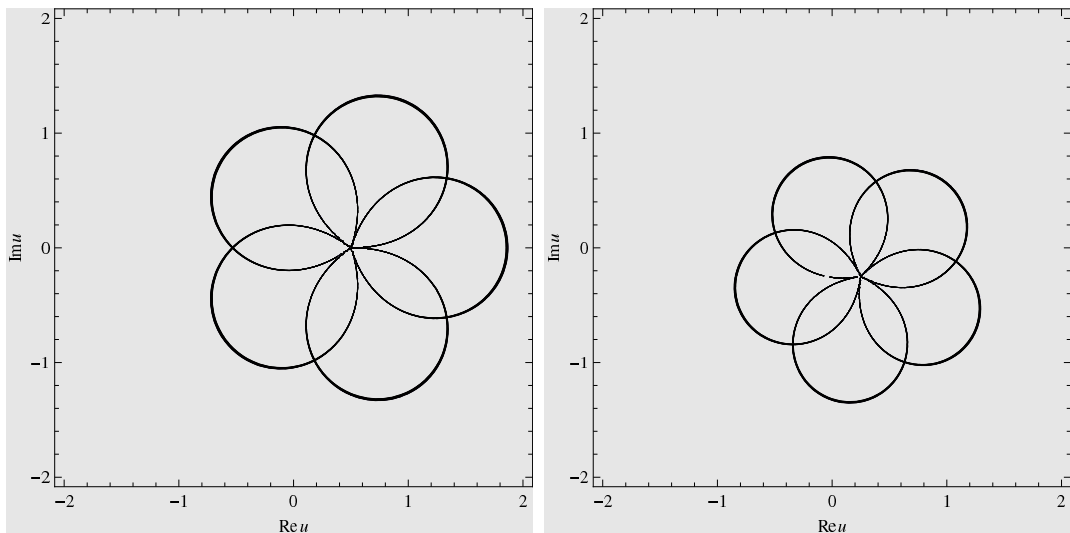


Figure 17: Single trajectory for the rational solution of $\mathcal{H}_{1/3}^+$ with $\text{Im } \zeta_0 = 1$: (a) \mathcal{PT} -symmetric solutions for the values as specified in figure 15, (b) Broken \mathcal{PT} -symmetric solutions for the values as specified in figure 16.

Potentially there are of course many more possible values for ε to be considered. We conclude here just by presenting two more examples with ε being an integer, as these are the most common deformations usually considered. For these values we obtain yet

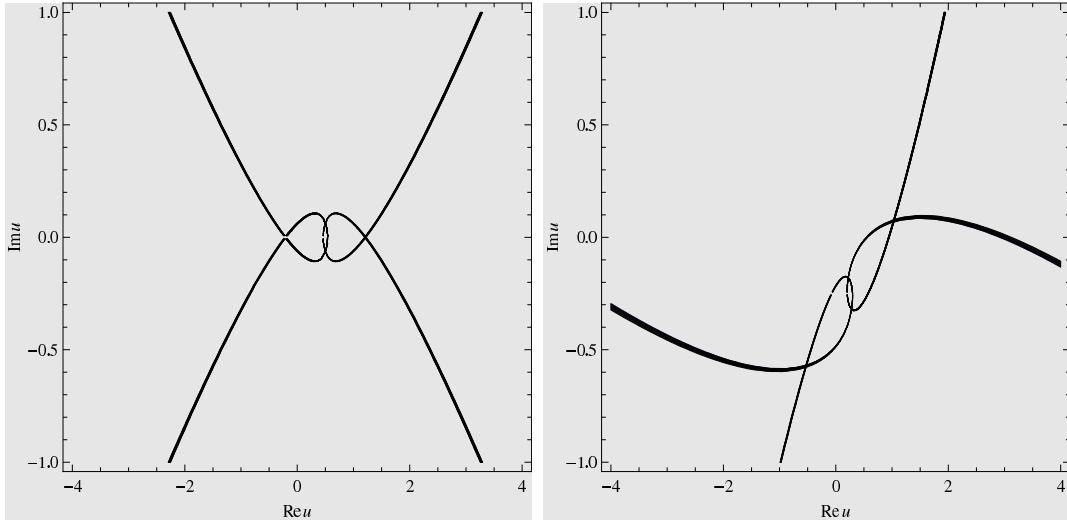


Figure 18: Single trajectory for the rational solution for of \mathcal{H}_3^+ with $\text{Im } \zeta_0 = 1$: (a) \mathcal{PT} -symmetric solutions for $A = 1/2$, $c = 1$, $\beta = 2$ and $\gamma = 3$, (b) Broken \mathcal{PT} -symmetric solutions for $A = 1/4(1 - i)$, $c = 1$, $\beta = 2 + 2i$ and $\gamma = 3$.

another type of characteristics as more and more branches have to be taken into account for increasing ε . In figure 18 and 19 we depict all branches for the trajectory with $\text{Im } \zeta_0 = 1$ for $\varepsilon = 3$ and $\varepsilon = 6$, respectively.

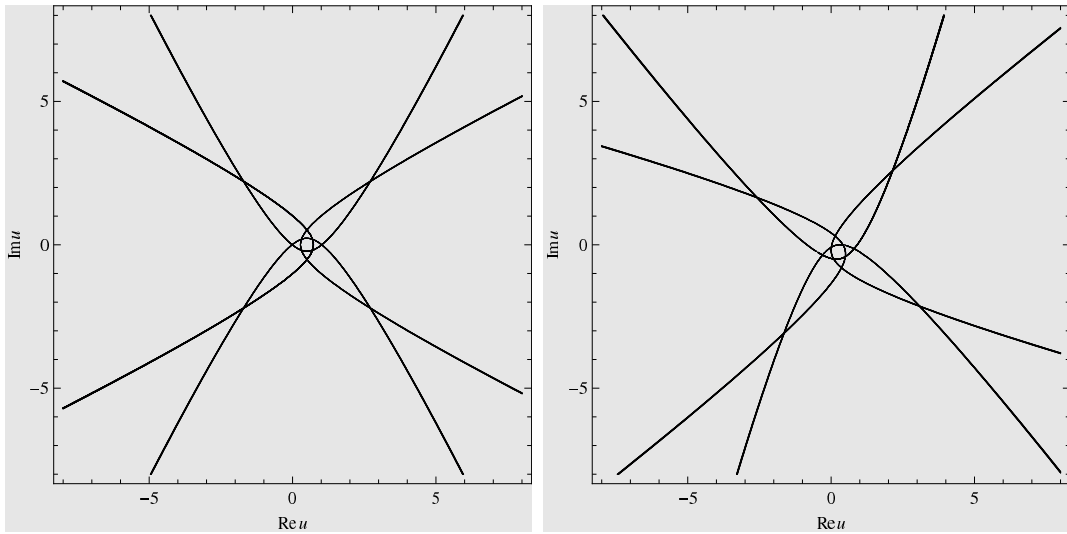


Figure 19: Single trajectory for the rational solution for of \mathcal{H}_6^+ with $\text{Im } \zeta_0 = 1$: (a) \mathcal{PT} -symmetric solutions for $A = 1/2$, $c = 1$, $\beta = 2$ and $\gamma = 3$, (b) Broken \mathcal{PT} -symmetric solutions for $A = 1/4(1 - i)$, $c = 1$, $\beta = 2 + 2i$ and $\gamma = 3$.

We observe some intricate winding behaviour near the fixed point, which, however, is not asymptotic in these cases. As is apparent from the solution (3.7) the trajectories diverge to infinity into various directions depending on the chosen Riemann sheet. Evidently the number of these asymptotes grows with increasing ε . Breaking the \mathcal{PT} -symmetry will only

distort the trajectories, giving rise to new directions of the asymptotes, but not changing their numbers.

3.1.2 Trigonometric/hyperbolic solutions

As in the non-deformed case we assume next the factorization $P(u) = (u - A)^2(u - B)$, which will impose once more the constraints (2.14). Also in this case we can compute (3.5) numerically.

Again we supplement our numerical findings by some analytical results. We can predict once more the lines for which $\zeta_0 = 0$ explicitly following the arguments of the previous subsection, with the difference that we have to take the limit to either the point A or B . For the angle of lines near the point A we find

$$\theta_A^{(n,m,\pm)} = \frac{\pi}{2(\varepsilon - 1)} [1 - \varepsilon + 4(n - m) - 4m\varepsilon] + \frac{1}{\varepsilon - 1} \arg(A - B) + \frac{1}{\varepsilon - 2} \arg(\pm\lambda_\varepsilon) \quad (3.10)$$

whereas for the angle of lines near the point B we compute

$$\theta_B^{(n,m,\pm)} = \frac{\pi}{2} (\varepsilon - 1 - 4n) + (1 + \varepsilon)2\pi m + (\varepsilon - 1) \arg(B - A) - \arg(\pm\lambda_\varepsilon). \quad (3.11)$$

We depict some specific examples with different characteristics in the figures 20 to 24.

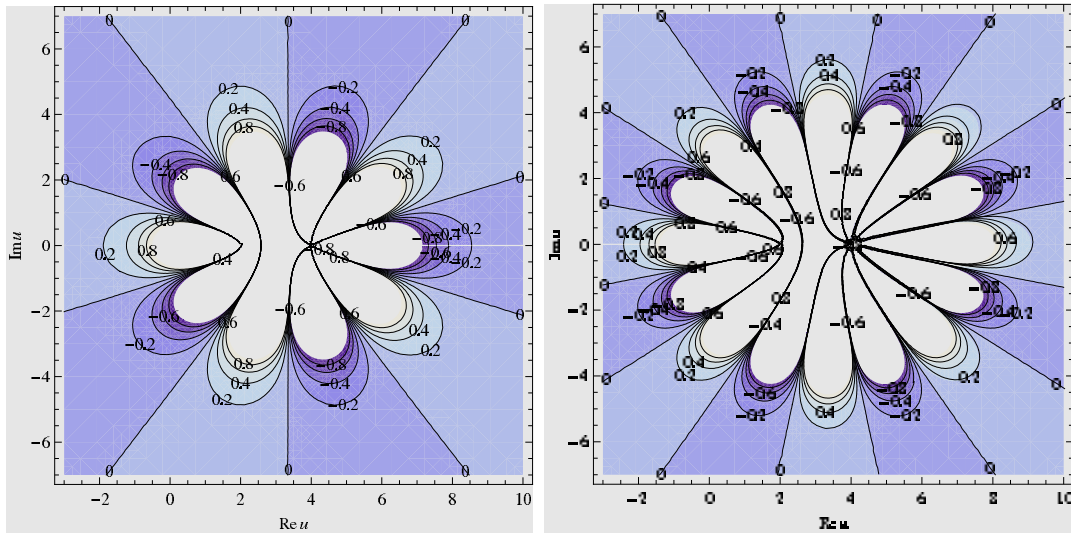


Figure 20: Complex \mathcal{PT} -symmetric trigonometric/hyperbolic solutions of the deformed KdV equation with $A = 4, B = 2, c = 1, \beta = 2$ and $\gamma = 3$ for (a) $\mathcal{H}_{-1/2}^+$ and (b) $\mathcal{H}_{-2/3}^+$.

In figure 20 we recognize a similar characteristic behaviour as for the rational solution of the same model depicted in figure 13. Roughly the portrait 20 corresponds to 13 with the difference that the single flower centre in the rational case situated as A has been pulled apart to the two points A and B in the trigonometric one. The overall effect is that some of trajectories separated in the rational case in different wedges are joint in the trigonometric/hyperbolic case. To illustrate this we have extracted one single trajectory in figure 21. We observe a similar behaviour for the entire sequel parameterized by $\varepsilon =$

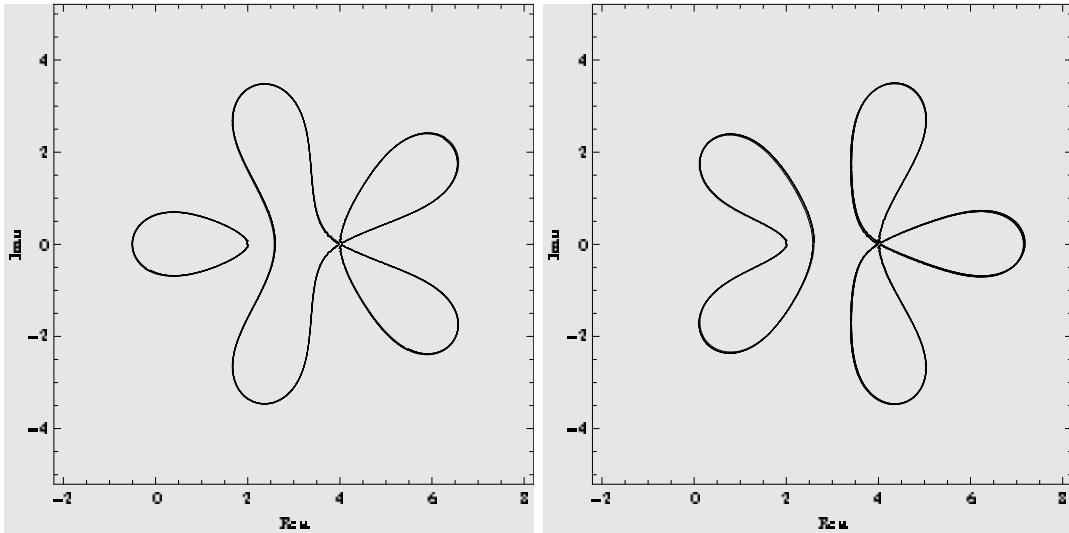


Figure 21: Single trajectory for the complex \mathcal{PT} -symmetric trigonometric/hyperbolic solutions of the deformed KdV equation for $\mathcal{H}_{-1/2}^+$ with the same values as specified in figure 20 for (a) $\text{Im}\zeta_0 = 1$ and (b) $\text{Im}\zeta_0 = -1$.

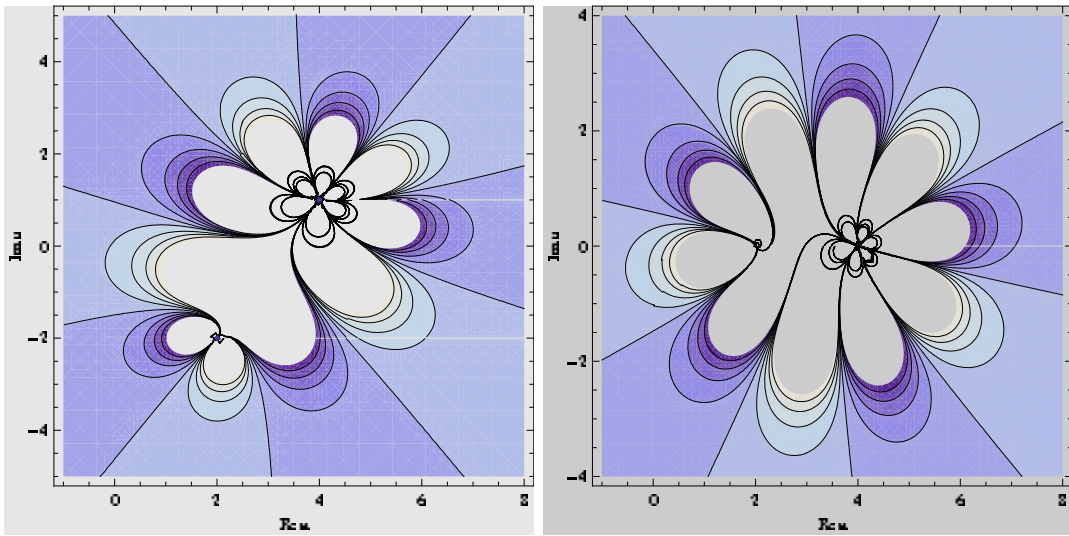


Figure 22: Broken \mathcal{PT} -symmetric trigonometric/hyperbolic solutions of the deformed KdV equation $\mathcal{H}_{-1/2}^+$: (a) Spontaneously broken \mathcal{PT} -symmetry with $A = 4 + i$, $B = 2 - 2i$, $c = 1$, $\beta = 3/10$ and $\gamma = 3$; (b) broken \mathcal{PT} -symmetry with $A = 4$, $B = 2$, $c = 1$, $\beta = 3/10$ and $\gamma = 3 + i$.

$-n/(n + 1)$ with $n = 1, 2, \dots$. Notice also that unlike as in the case $\varepsilon = 1$ there is no distinction between a periodic and an asymptotically constant solution.

Having enough free parameters available we can now break the symmetry for this solution also spontaneously or completely as illustrated in figure 22. In both cases we observe that the amount of wedges remains unchanged, the symmetry about the real axis is lost and the winding around the fixed points becomes more intricate. In addition, trajectories from certain wedge regions connect in different ways, e.g. in figure 20 we

observe a connected trajectory in the two light shaded wedge region to the left of the vertical as can also be seen in figure 21. Such type of trajectories do not exist in the broken case as we can observe in figure 22. We note that instead trajectories from the light shaded region in the upper half plane connect to a dark shaded region in the lower half plane to the left of the corresponding light shaded region in the unbroken case.

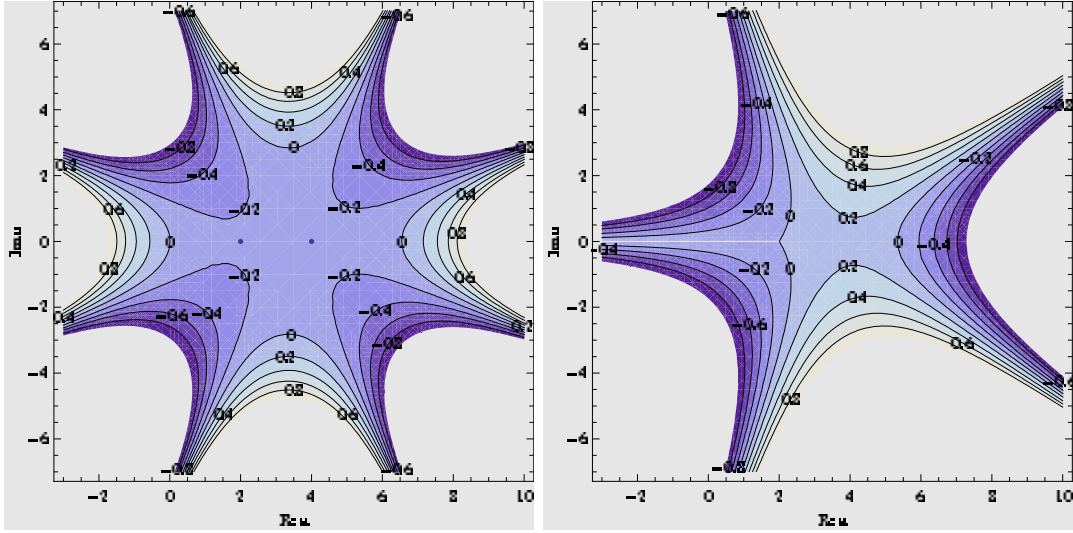


Figure 23: Complex PT -symmetric trigonometric/hyperbolic solutions of the deformed KdV equation with $A = 4$, $c = 1$, $\beta = 2$ and $\gamma = 3$ for (a) \mathcal{H}_{-2}^+ and (b) \mathcal{H}_{-3}^+ .

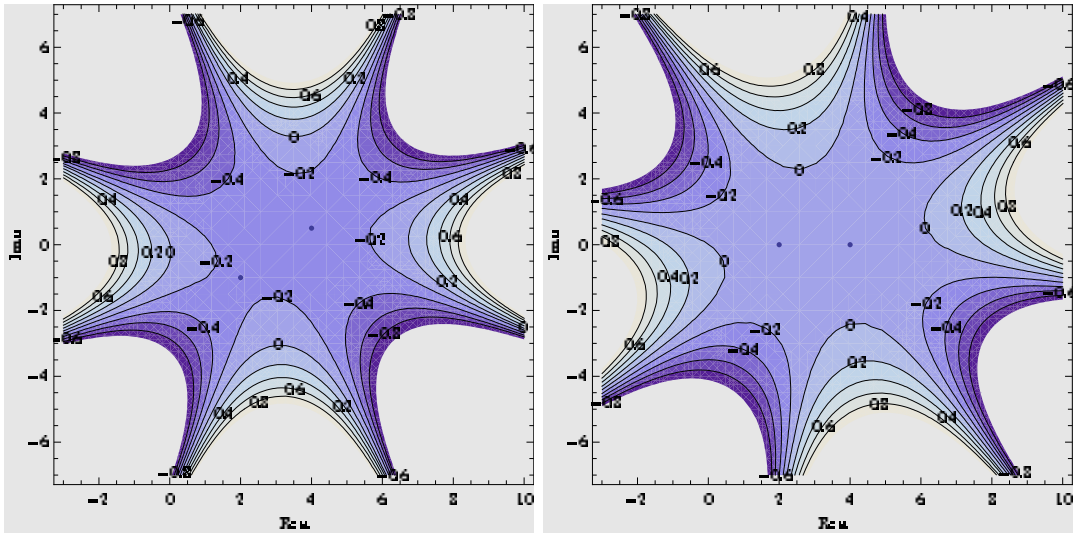


Figure 24: Broken PT -symmetric trigonometric/hyperbolic solutions of the deformed KdV equation for \mathcal{H}_{-2}^+ : (a) Spontaneously broken PT -symmetry with $A = 4 + i/2$, $B = 2 - i$, $c = 1$, $\beta = 3/10$ and $\gamma = 3$; (b) broken PT -symmetry with $A = 4$, $B = 2$, $c = 1$, $\beta = 3/10$ and $\gamma = 3 + 4i$.

Comparing next the solutions for $\varepsilon \in \mathbb{R}^-$ we observe in figure 23a a similar transformation from the rational to the trigonometric/hyperbolic case as for the previous example.

Again we find that the rational solution resembles this solution for the same values of the deformation parameters, with the difference that the characteristic behaviour around the point A in the rational case has been distorted to the points A and B .

The broken \mathcal{PT} -symmetric case for this model is presented in figure 24. In panel (a) we depict the spontaneously broken \mathcal{PT} -symmetric scenario for \mathcal{H}_{-2}^+ , observing that the symmetry is lost since the trajectories rotate together with the two fixed points. The \mathcal{PT} -symmetry is completely broken in the presentation in 24b for the same model. Having kept the values for the fixed points, we note that in this case the orbits rotate around them.

We have investigated also other models observing similar patterns, which we will however not present here.

3.1.3 Elliptic solutions

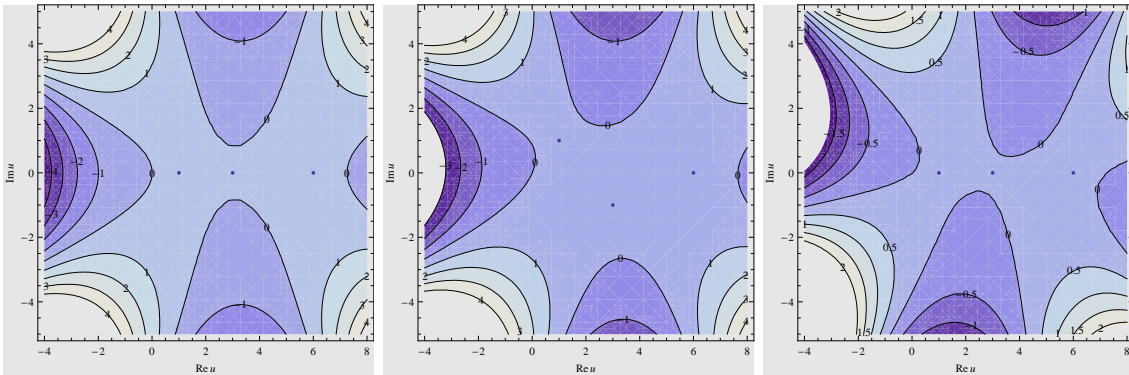


Figure 25: Elliptic solutions for \mathcal{H}_{-2}^+ : (a) \mathcal{PT} -symmetric with $A = 1$, $B = 3$, $C = 6$, $\beta = 3/10$, $\gamma = -3$ and $c = 1$; (b) spontaneously broken \mathcal{PT} -symmetry with $A = 1 + i$, $B = 3 - i$, $C = 6$, $\beta = 3/10$, $\gamma = -3$ and $c = 1$; (c) broken \mathcal{PT} -symmetry with $A = 1$, $B = 3$, $C = 6$, $\beta = 3/10$, $\gamma = -3 + 4i$ and $c = 1$.

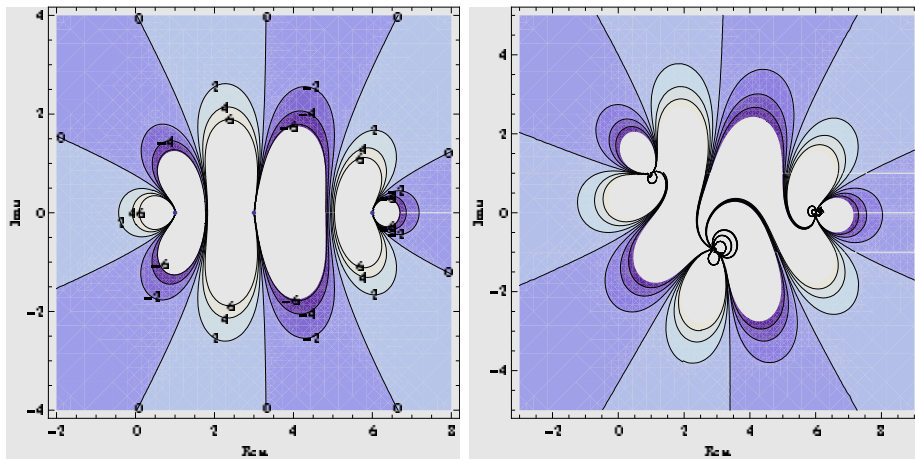


Figure 26: Elliptic solutions for $\mathcal{H}_{-1/2}^+$: (a) \mathcal{PT} -symmetric with $A = 1$, $B = 3$, $C = 6$, $\beta = 3/10$, $\gamma = -3$ and $c = 1$; (b) spontaneously broken \mathcal{PT} -symmetry with $A = 1 + i$, $B = 3 - i$, $C = 6$, $\beta = 3/10$, $\gamma = -3$ and $c = 1$.

Proceeding just as in the undeformed case we specify next $P(u) = (u-A)(u-B)(u-C)$, which imposes the constraints (2.22) and (2.23), thus leaving two constants free. We present here only the results for the cases $\varepsilon = -2$ and $\varepsilon = -1/2$ in the figures 25 and 26, respectively.

In all three possible scenarios we observe a similar qualitative behaviour as for the trigonometric/hyperbolic solutions of the previous subsection with the difference that we have three instead of two fixed points.

3.2 The $\mathcal{H}_\varepsilon^-$ -models

Let us now turn to the second type of deformation. In order to construct the solutions we proceed in a similar manner as in the previous case. Integrating now twice the second equation in equation (3.3) we obtain

$$u_\zeta^2 = \frac{2}{\gamma} \left(\kappa_2 + \kappa_1 u + \frac{c}{2} u^2 - \beta \frac{i^\varepsilon}{(1+\varepsilon)(2+\varepsilon)} u^{2+\varepsilon} \right) =: \lambda Q(u), \quad (3.12)$$

where

$$\lambda = -\frac{2\beta i^\varepsilon}{\gamma(1+\varepsilon)(2+\varepsilon)}. \quad (3.13)$$

A crucial difference between $\mathcal{H}_\varepsilon^+$ and $\mathcal{H}_\varepsilon^-$ is that unlike as the polynomial $P(u)$, which was of fixed order 3, the order of $Q(u)$ depends on ε , meaning that we have more and more possibilities to factorize it for growing ε . For instance, for a given integer value $n \in \mathbb{N}_0$ the factorization of $Q(u)$ as

$$Q(u) = (u - A_1)^{\varepsilon+2-n} \prod_{i=1}^n (u - A_{i+1}), \quad (3.14)$$

admits solutions provided $n - 2 \leq \varepsilon \leq n + 1$ and $\varepsilon \in \mathbb{N}$. This allows of course for yet another infinity of possibilities.

When $\kappa_1 = \kappa_2 = 0$ we can find a closed solution valid for all ε by integrating (3.12) and solving it for u

$$u(\zeta) = \left(\frac{c(\varepsilon+1)(\varepsilon+2)}{i^\varepsilon \beta \left[\cosh \left(\frac{\sqrt{c\varepsilon}(\zeta-\zeta_0)}{\sqrt{\gamma}} \right) + 1 \right]} \right)^{1/\varepsilon}. \quad (3.15)$$

The generic scenario does not yield such a simple answer.

3.2.1 \mathcal{H}_2^-

This case is especially interesting as it corresponds to a complex version of the modified KdV-equation. Specifying (3.14) for instance as $Q(u) = (u-A)^3(u-B)$ we can factorize the polynomial in (3.12) with the choice

$$\kappa_1 = -\frac{2c^{3/2}}{3\sqrt{-\beta}}, \quad \kappa_2 = -\frac{c^2}{4\beta}, \quad A = -\frac{B}{3} \quad \text{and} \quad B = -\frac{3\sqrt{c}}{\sqrt{-\beta}}. \quad (3.16)$$

Notice that this fixes all the boundary conditions for a given model. Solving (3.12) then yields a rational solution for the second equation in (3.3)

$$u(\zeta) = \sqrt{-\frac{c}{\beta} \frac{2c\zeta^2 - 9\gamma}{3\gamma + 2c\zeta^2}}. \quad (3.17)$$

As is well know for the real case one may construct solutions for the KdV-equation from those of the modified KdV-equation by means of a Miura transformation. We expect this also to hold for their complex versions. Indeed, using the transformation of the form

$$u_{\text{KdV}}(\zeta) = \sqrt{\frac{6\gamma}{\beta}} u_\zeta - u^2 \quad (3.18)$$

yields the rational solution of the KdV-equations (2.12) from (3.17) when we identify $\zeta_0 = i\sqrt{3\gamma/2c}$ therein.

Assuming in (3.14) instead $Q(u) = (u - A)^2(u - B)(u - C)$ we can factorize the polynomial in (3.12) with the constraints

$$\kappa_1 = \frac{\beta C^2(\vartheta - 5C\beta) + 9c(\vartheta - 3C\beta)}{81\beta}, \quad \kappa_2 = \frac{C(2\vartheta - C\beta)(C\beta + \vartheta)^2}{324\beta^2}, \quad (3.19)$$

$$A = -\frac{1}{2}(B + C) \quad \text{and} \quad B = \frac{2\vartheta - C\beta}{3\beta} \quad (3.20)$$

where we abbreviated $\vartheta := \sqrt{2}\sqrt{-\beta(\beta C^2 + 9c)}$. Notice that in this case one constant remains free. The integration of (3.12) yields in this case a trigonometric solution, which, using the same Miura transformation (3.18), may also be converted into a solution of the KdV-equations.

3.2.2 \mathcal{H}_4^-

In this case the polynomial of the right hand side of (3.12) is of sixth order. We present here just one very symmetric solution by assuming a factorization of the form $Q(u) = u^2(u^2 - B^2)(u^2 - C^2)$, which is possible with the simple choice

$$\kappa_1 = \kappa_2 = 0, \quad B = iC \quad \text{and} \quad C^4 = \frac{15c}{\beta}. \quad (3.21)$$

Thus we have made contact with the solution (3.15). Parameterizing $B = r_B e^{i\theta_B}$ and $\lambda = r_\lambda e^{i\theta_\lambda}$ the eigenvalues of the Jacobian when linearized about $u = 0$ are easily computed to

$$j_1 = \pm i\sqrt{r_\lambda} r_B^2 \exp\left[\frac{i}{2}(4\theta_B + \theta_\lambda)\right] \quad \text{and} \quad j_2 = \mp i\sqrt{r_\lambda} r_B^2 \exp\left[-\frac{i}{2}(4\theta_B + \theta_\lambda)\right]. \quad (3.22)$$

This means for the \mathcal{PT} -symmetric solution we always obtain two real degenerate eigenvalues and therefore a star node at $u = 0$. For the positive square root in (3.12) with $B = \pm(15c/\beta)^{1/4}$ or with $B = \pm i(15c/\beta)^{1/4}$ the node is stable or unstable, respectively. The stability property is reversed for the negative square root. Taking the branch cuts at $\text{Im } u = 0$, $\text{Re } u = 0$, $\text{Im } u = \text{Re } u$ and $\text{Im } u = -\text{Re } u$ into account we obtain closed curves. The four zeros of $Q(u)$, i.e. $\pm(15c/\beta)^{1/4}$, $\pm i(15c/\beta)^{1/4}$, are surrounded by the trajectories. All these features can be seen in figure 27a. We may also tune the coupling constants in such a way that $4\theta_B + \theta_\lambda = 0$, which by (3.22) implies that the fixed point at the origin should become a centre. Indeed, for a specific choice we observe this in figure 27b. Apart from the origin, the remaining four fixed points are now situated outside of the trajectories.

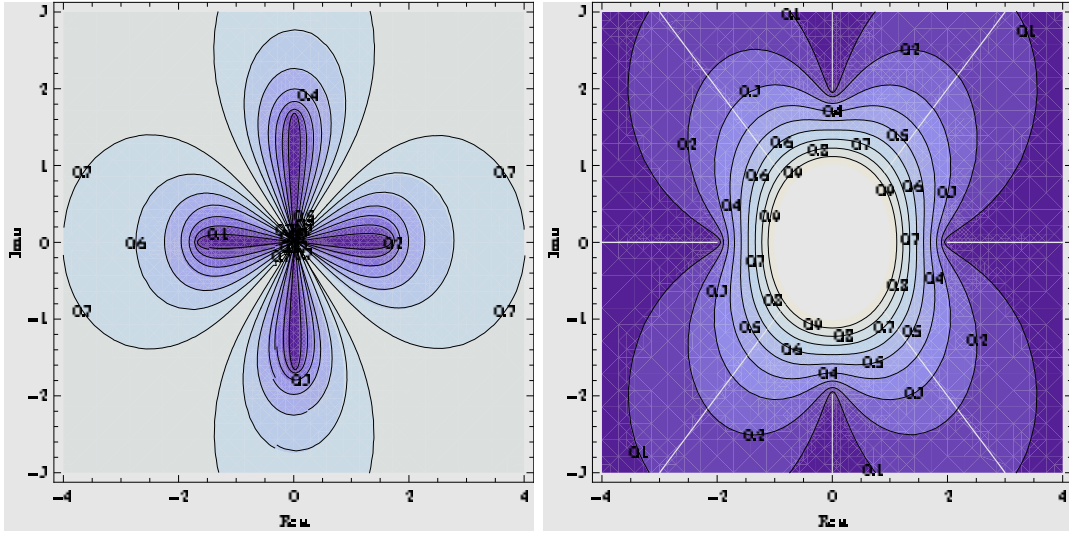


Figure 27: \mathcal{PT} -symmetric solutions for \mathcal{H}_4^- : (a) Star node at the origin for $c = 1$, $\beta = 2$, $\gamma = 1$ and $B = (15/2)^{1/4}$; (b) centre at the origin for $c = 1$, $\beta = 1$, $\gamma = -1$ and $B = (15/2)^{1/4}$.

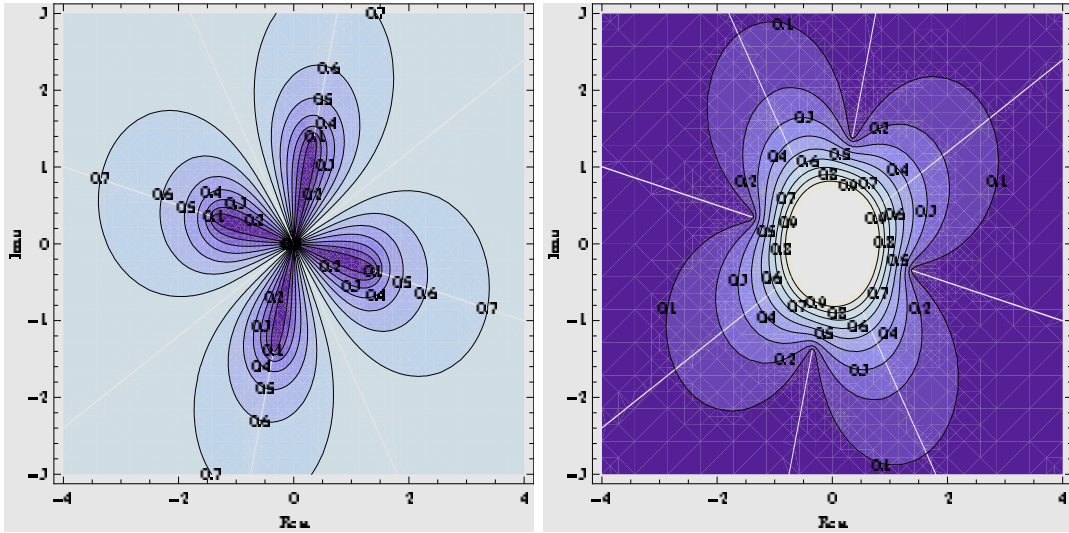


Figure 28: Broken \mathcal{PT} -symmetric solution for \mathcal{H}_4^- : (a) Star node at the origin for $c = 1$, $\beta = 2 + i3$, $\gamma = 1$ and $B = (15/2 + i3)^{1/4}$; (b) centre at the origin for $c = 1$, $\beta = 2 + i3$, $\gamma = -1$ and $B = (30/13 - i45/13)^{1/4}$.

Since we have no free parameter left in our factorization this solution can not be broken spontaneously. A complete breaking is carried out by complexifying β or γ . When choosing $\text{Im } \beta \neq 0$ we can still achieve in (3.22) that $4\theta_B + \theta_\lambda = \pm\pi$, such that the star node nature of the fixed point is preserved despite the fact that the \mathcal{PT} -symmetry is lost. For a particular choice this behaviour is depicted in figure 28a. More surprising is the fact that we can also achieve that $4\theta_B + \theta_\lambda = 0$ in the broken case. This means the eigenvalues in (3.22) are purely imaginary and the fixed point at the origin is a centre. We depict this possibility in figure 28b. This means we have closed trajectories even in the \mathcal{PT} -symmetrically broken

case.

In contrast for $\text{Im}\gamma \neq 0$ the eigenvalues j_i will become complex and the fixed point at the origin turns into an unstable or stable focus. Taking the branch cut structure into account we observed this behaviour in figure 29a for $\beta \in \mathbb{R}$, $\gamma \in \mathbb{C}$ and in figure 29b for $\beta \in \mathbb{C}$, $\gamma \in \mathbb{C}$.

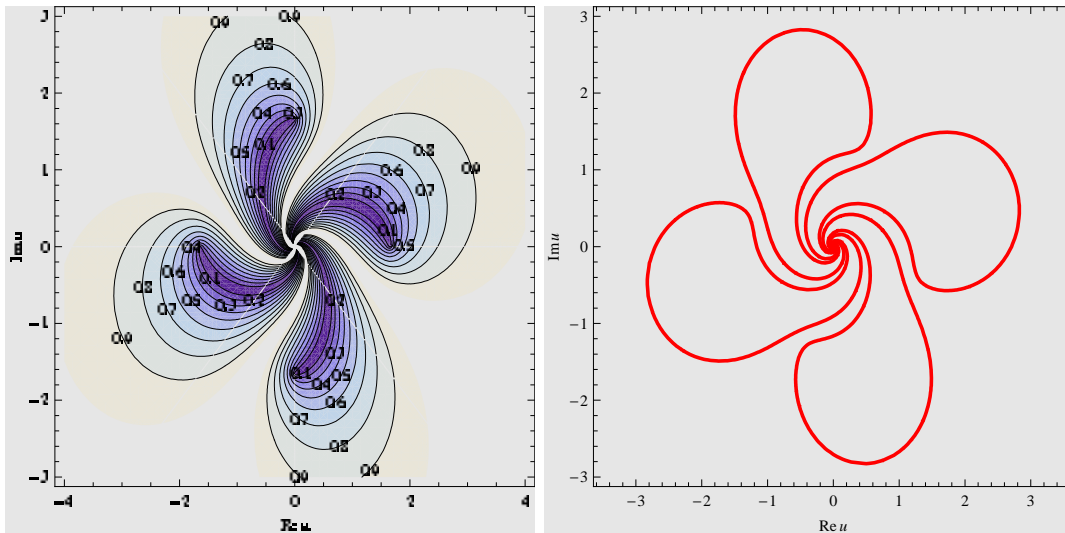


Figure 29: Broken \mathcal{PT} -symmetric solution for \mathcal{H}_4^- : (a) focus at the origin for $c = 1$, $\beta = 2$, $\gamma = 1 + i3$ and $B = (15/2)^{1/4}$; (b) focus at the origin for $\text{Im}\zeta_0 = 0.8$, $c = 1$, $\beta = 2 + i3$, $\gamma = -1 + i2$ and $B = (30/13 - i45/13)^{1/4}$.

Once again we observed that when identifying a coupling constant as a bifurcation parameter, the origin undergoes a Hopf bifurcation.

Making once more the identification $u \rightarrow x$ and $\zeta \rightarrow t$ for our traveling wave equation together with the identification

$$\kappa_1 = 0, \quad \kappa_2 = \gamma E, \quad \text{and} \quad \beta = \gamma g(1 + \varepsilon)(2 + \varepsilon) \quad (3.23)$$

equation (3.12) converts into the classical deformation of the harmonic oscillator

$$H = E = \frac{1}{2}p^2 - \frac{c}{2\gamma}x^2 + gx^2(ix)^\varepsilon. \quad (3.24)$$

Setting furthermore $c = 0$, which in our setting corresponds to a static solution, we obtain precisely the potential treated in the seminal paper by Bender and Boettcher [4].

4. Complex coupled nonlinear wave equation of Ito type

It is known for some time that the Korteweg-deVries field $u(x, t)$ may be coupled to a nonlinear field $v(x, t)$ without destroying the integrability of the newly constructed system. This coupling is carried out by the introduction of an additional dispersion term involving

the second field $v(x, t)$ and the assumption of a specific form of the evolution equation for this field. The coupled system describing this type of scenario acquires the general form

$$u_t + \alpha v v_x + \beta u u_x + \gamma u_{xxx} = 0, \quad \alpha, \beta, \gamma \in \mathbb{C}, \quad (4.1)$$

$$v_t + \delta(uv)_x + \phi v_{xxx} = 0, \quad \delta, \phi \in \mathbb{C}. \quad (4.2)$$

Imposing the constraints $\beta = 3\gamma$, $\phi = 1$, $\delta = 3$ on the constants and leaving α , γ free, the Hirota method can be applied to establish that the system (4.1) and (4.2) possesses N-soliton solutions [40]. When selecting in addition $\gamma = -1/2$ as in [41] or $\alpha = -2$, $\beta = -6$, $\gamma = -1$, $\delta = -2$ and $\phi = 0$ as in [42], it was established in both cases that the system possesses infinitely many charges. For $\phi = 0$ the system (4.1) and (4.2) was shown to possess soliton solutions of cusp type [43]. Notice also that when complexifying the KdV-field in (2.2) as $u_{\text{KdV}} \rightarrow u + iv$ we obtain the system (4.1) and (4.2) for the special choice $\alpha = -\beta_{\text{KdV}}$, $\beta = \beta_{\text{KdV}}$, $\gamma = \gamma_{\text{KdV}}$, $\delta = \beta_{\text{KdV}}$ and $\phi = \gamma_{\text{KdV}}$. In the following we will mainly discuss the case $\phi = 0$, such that even the real case of (4.1) and (4.2) is distinct from the complexified version of the KdV equation.

It is straightforward to verify that for the choice $\delta = \alpha$ the system of equations (4.1) and (4.2) results from a variation of a Hamiltonian whose density is given by

$$\mathcal{H}_I = -\frac{\alpha}{2}uv^2 - \frac{\beta}{6}u^3 + \frac{\gamma}{2}u_x^2 + \frac{\phi}{2}v_x^2, \quad (4.3)$$

when using the variational derivative and time evolution in the standard way

$$w_t = \frac{\partial}{\partial x} \left(\sum_{n=0}^{\infty} (-1)^n \frac{d^n}{dx^n} \frac{\partial \mathcal{H}_I}{\partial w_{nx}} \right)_x \quad \text{for } w = u, v. \quad (4.4)$$

The Hamiltonian resulting from the density (4.3) is manifestly \mathcal{PT} -symmetric as it remains invariant under a simultaneous parity transformation and time reversal which may be realised in four alternative ways as

$$\mathcal{PT}_{++} : x \mapsto -x, t \mapsto -t, i \mapsto -i, u \mapsto u, v \mapsto v \quad \text{for } \alpha, \beta, \gamma, \phi \in \mathbb{R}, \quad (4.5)$$

$$\mathcal{PT}_{+-} : x \mapsto -x, t \mapsto -t, i \mapsto -i, u \mapsto u, v \mapsto -v \quad \text{for } \alpha, \beta, \gamma, \phi \in \mathbb{R}, \quad (4.6)$$

$$\mathcal{PT}_{-+} : x \mapsto -x, t \mapsto -t, i \mapsto -i, u \mapsto -u, v \mapsto v \quad \text{for } i\alpha, i\beta, \gamma, \phi \in \mathbb{R}, \quad (4.7)$$

$$\mathcal{PT}_{--} : x \mapsto -x, t \mapsto -t, i \mapsto -i, u \mapsto -u, v \mapsto -v \quad \text{for } i\alpha, i\beta, \gamma, \phi \in \mathbb{R}, \quad (4.8)$$

depending on whether we choose the fields u, v to be \mathcal{PT} -symmetric or anti-symmetric. All possibilities ensure that $\mathcal{PT}_{ij} : \mathcal{H}_I \mapsto \mathcal{H}_I$ holds with $i, j \in \{+, -\}$. First we will exploit these possibilities to explain the reality of the energies and in section 5 we use them to define new physically feasible models.

4.1 \mathcal{PT} -symmetric, spontaneously broken and broken solutions

As usual in this context we assume that the fields acquire the form of a traveling wave $u(x, t) = u(\zeta)$ and $v(x, t) = v(\zeta)$ with $\zeta = x - ct$. In [44] it was shown for the case $\phi = 0$ that the possibility to have only one field to be a traveling wave and not the other is

inconsistent. We extrapolate here without rigorous proof that this assumption can be made without loss of generality even in other cases. Let us briefly recall how these equations may be solved in a systematic way. To begin with we integrate (4.1) and (4.2) to

$$-cu + \frac{\alpha}{2}v^2 + \frac{\beta}{2}u^2 + \gamma u_{\zeta\zeta} = \kappa_1, \quad (4.9)$$

$$-cv + \alpha uv = \kappa_2, \quad (4.10)$$

with integration constants κ_1, κ_2 . In the following we always exclude the case $\kappa_2 = 0$ as this implies the vanishing of the new field $v = 0$, which means a reduction to the deformed KdV equation, or a constant KdV-field $u = \alpha/c$. Multiplying (4.9) by u_{ζ} , using (4.10) to replace v by u in (4.9), we can integrate once more and obtain

$$u_{\zeta}^2 = \frac{2}{\gamma} \left(\kappa_3 + \kappa_1 u + \frac{c}{2} u^2 - \frac{\beta}{6} u^3 + \frac{\kappa_2^2}{2} \frac{1}{\alpha u - c} \right). \quad (4.11)$$

This equation is difficult to solve directly, but following [43] we trade the u field for the v field with

$$u = \frac{c}{\alpha} + \frac{\kappa_2}{\alpha v} \quad \text{and} \quad u_{\zeta} = -\frac{\kappa_2}{\alpha v^2} v_{\zeta} \quad (4.12)$$

and obtain

$$v_{\zeta}^2 = -\frac{v}{3\alpha\gamma\kappa_2^2} \sum_{k=0}^4 a_k v^k, \quad (4.13)$$

where

$$\begin{aligned} a_0 &= \beta\kappa_2^3, & a_1 &= 3c\kappa_2^2(\beta - \alpha), & a_2 &= 3\kappa_2(\beta c^2 - 2\alpha c^2 - 2\alpha^2\kappa_1), \\ a_3 &= c^3(\beta - 3\alpha) - 6\alpha^2(c\kappa_1 + \alpha\kappa_3), & a_4 &= -3\alpha^3\kappa_2. \end{aligned} \quad (4.14)$$

At first sight this looks even less encouraging than (4.11). However, now the right hand side is a polynomial and in case we can factorize the sum $\sum_{k=0}^4 a_k v^k$ into some convenient form we may be able to integrate (4.13) similarly as in the previous section. Up to one integration the solution is therefore

$$\pm\sqrt{\lambda}(\zeta - \zeta_0) = \int dv \frac{1}{\sqrt{R(v)}}, \quad (4.15)$$

with $\lambda = \alpha^2/\gamma\kappa_2$ and $\lambda R(v)$ corresponding to the right hand side of (4.13). We note that not all conceivable assumptions for the sum will lead to meaningful or nontrivial solutions. Taking for instance $R(v) = v^4(A + v)$ or $R(v) = v^3(A + v)(B + v)$ with some unknown constants A and B leads in both cases to $\kappa_2 = 0$ or $\beta = 0$, which we exclude for the above mentioned reasons.

When demanding vanishing asymptotic boundary conditions for the u -field and its derivatives, the relations (4.9) and (4.11) imply that we satisfy the additional constraints

$$\lim_{\zeta \rightarrow \pm\infty} u, u_{\zeta}, u_{\zeta\zeta} = 0 \quad \Rightarrow \quad \kappa_1 = \frac{\alpha\kappa_2^2}{2c^2}, \quad \kappa_3 = \frac{\kappa_2^2}{2c}, \quad \lim_{\zeta \rightarrow \pm\infty} v = -\frac{\kappa_2}{c}. \quad (4.16)$$

4.1.1 Type I solutions

The simplest possible factorization for the sum in (4.13) is $R(v) = v(v - A)^4$, which holds up to the constraints

$$\begin{aligned} \kappa_1 &= \frac{c^2 (2\beta\alpha - 9\alpha^2 - \beta^2)}{16\alpha^2\beta}, & \kappa_2 &= \frac{3\sqrt{3}c^2(\alpha - \beta)^2}{16\alpha^{3/2}(-\beta)^{3/2}}, \\ \kappa_3 &= \frac{c^3(3\alpha - \beta)(9\alpha^2 - 6\beta\alpha + 5\beta^2)}{96\alpha^3\beta^2} & \text{and} & \quad A = \frac{\sqrt{3}c(\beta - \alpha)}{4\alpha^{3/2}\sqrt{-\beta}}. \end{aligned} \quad (4.17)$$

For a given specific model, i.e. fixed $\alpha, \beta, \gamma, \phi$, this means that all remaining free parameters are fixed. Vanishing asymptotic boundary conditions for u require by the first two equations in (4.16) only *one* further relation $\beta = -3\alpha$, despite the fact that one has to solve *two* constraining equations. Solving (4.15) for the given factorization yields

$$\zeta - \zeta_0 = \pm \frac{1}{A\sqrt{\lambda}} \left[\frac{\operatorname{arctanh}\left(\frac{\sqrt{v}}{\sqrt{A}}\right)}{\sqrt{A}} + \frac{\sqrt{v}}{A - v} \right]. \quad (4.18)$$

First we focus on the real solution, which is obtained from (4.18) for $\lambda > 0$ and $0 < v < A$. A further solution is obtained when replacing in (4.18) the $\operatorname{arctanh}$ by arcoth , which produces a real solution for $0 < A < v$. Again we are faced with the problem that we are not able to extract from (4.18) the function $v(\zeta)$. Nonetheless, we can re-write (4.18) as

$$v(\zeta) = A + \frac{\sqrt{v(\zeta)}\sqrt{A}}{\operatorname{arctanh}\left(\frac{\sqrt{v(\zeta)}}{\sqrt{A}}\right) \pm A^{3/2}\sqrt{\lambda}(\zeta - \zeta_0)} \quad (4.19)$$

similarly as done in [43]. This is of course still not $v(\zeta)$, but this form is very useful to extract various types of information in an analytical manner. Simply by considering the functions on the right hand side of (4.19), we observe the asymptotic behaviour $\lim_{\zeta \rightarrow \pm\infty} v(\zeta) = A$. In principle this is already sufficient to extract the qualitative behaviour of $v(\zeta)$, since we also have assumed a simple factorization for the derivative of v in (4.13). We can, however, be more precise because the formulation (4.19) is also ideally suited to be solved numerically. In principle this possibility will become more powerful when considering more complicated scenarios. However, in these cases one encounters also more occurrences of the field v and it is not always obvious for which one the equation should be solved.

For the purpose of a numerical study we discretise the equations as $v_{n+1} = F(v_n)$ and subsequently solve them iteratively for given values of ζ . The fixed points $v_f(\zeta)$ of such discretised equations are known to be stable if and only if $|F'[v_f(\zeta)]| < 1$. We use this criterium to facilitate the numerical investigations. Concretely we solve the recursive equation

$$v_{n+1}(\zeta) = A + \frac{\sqrt{v_n(\zeta)}\sqrt{A}}{\operatorname{arctanh}\left(\frac{\sqrt{v_n(\zeta)}}{\sqrt{A}}\right) \pm A^{3/2}\sqrt{\lambda}(\zeta - \zeta_0)}, \quad (4.20)$$

which converges very rapidly to a precision of $\sim 10^{-5}$ typically already for less than 150 iterations. We proceed similarly for the solution when $0 < A < v$. In figure 30 we depict two types of cusp solutions obtained in this manner.

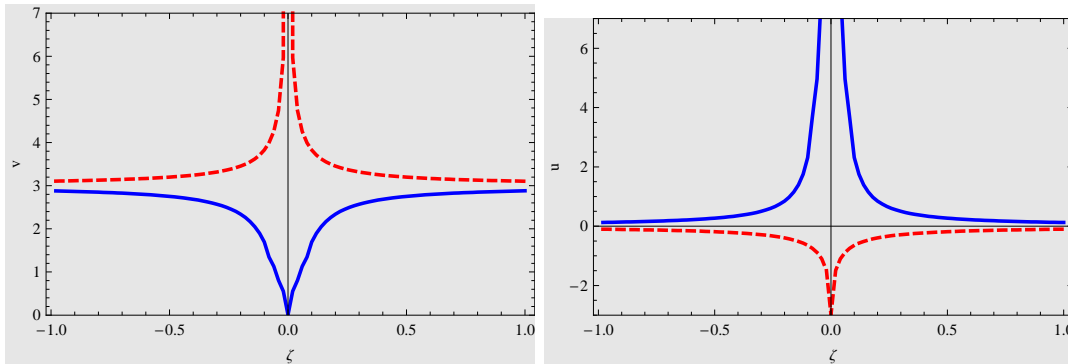


Figure 30: Cusp solutions with asymptotically vanishing boundary conditions for the u -field of the Ito type equation with $A = 3$, $c = 1$, $\alpha = -1/3$, $\beta = 1$, $\gamma = -1/27^2$ and $\zeta_0 = 0$: (a) v -field; (b) u -field.

In principle we could also proceed in this manner when taking complex initial conditions, but it is simpler to produce the contour plot in the way outlined at the beginning of section 3.1. For the same values of the parameters as in figure 30 we depict our results in figure 31, indicating as before the imaginary parts of ζ_0 on some particular trajectories.

As expected from (4.19) we observe in figures 31 that the complex solutions tend to the same asymptotic value as the real ones. The point A is an unstable focus in the \mathcal{PT} -symmetric and its broken version. In panel (b) more Riemann sheets are taken into account, revealing more substructure compared to panel (a). In the \mathcal{PT} -symmetric case we also observe the crucial feature that $v^*(\zeta) = v(-\zeta)$ and $u^*(\zeta) = u(-\zeta)$, which guarantees the reality of the energy as defined by the expression in (1.2).

4.1.2 Type II solutions

Next we introduce an additional parameter B and assume the factorization of the form $R(v) = v(v - A)^2(v - B)^2$, which imposes the four constraining equations

$$\kappa_1 = \frac{(\beta - 2\alpha)c^2}{2\alpha^2} + \frac{(A^2 + 4AB + B^2)\alpha}{2}, \quad (4.21)$$

$$\kappa_2 = \frac{2AB(A + B)\alpha^3}{c(\beta - \alpha)}, \quad (4.22)$$

$$\kappa_3 = \frac{2AB(A + B)^2\alpha^3}{c(\alpha - \beta)} + \frac{c^3(3\alpha - 2\beta)}{6\alpha^3} - \frac{c(A^2 + 4AB + B^2)}{2}, \quad (4.23)$$

$$A + B = \pm \frac{\sqrt{3}c(\alpha - \beta)}{2\alpha^{3/2}\sqrt{-\beta}}. \quad (4.24)$$

This means our five constants $\kappa_1, \kappa_2, \kappa_3, A, B$ are constrained by four equations, such that one of them remains free and thus allows us to adjust for some desired boundary conditions.

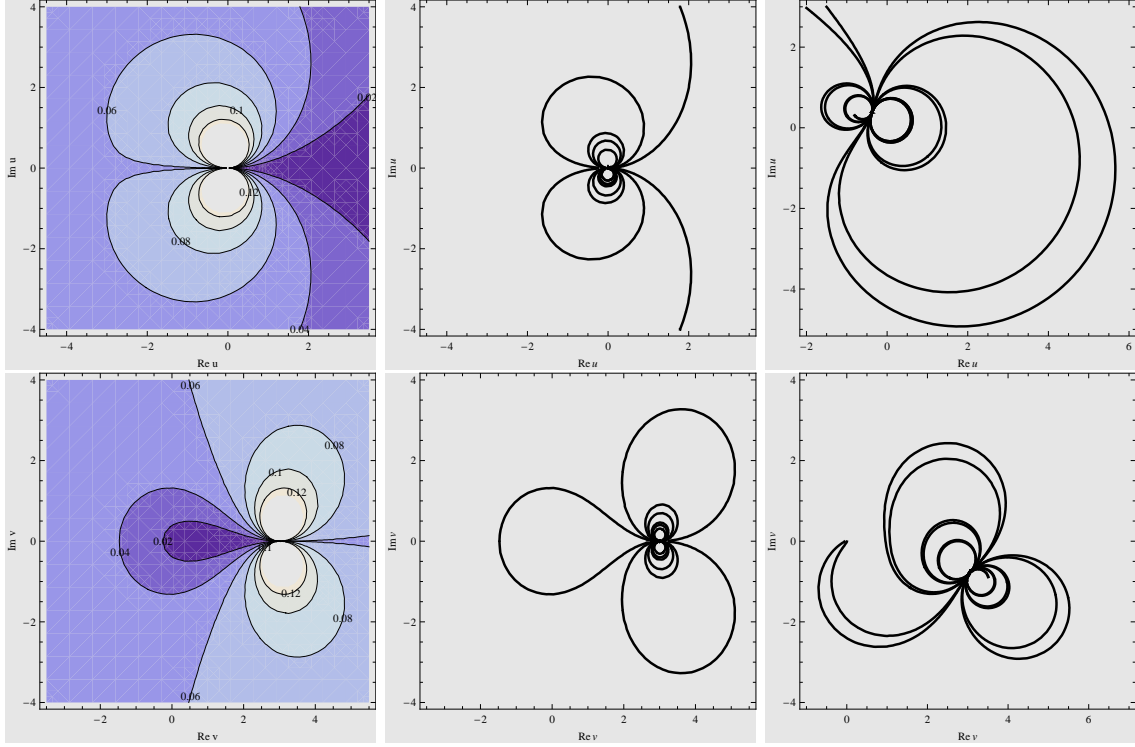


Figure 31: Complex type I solutions with asymptotically vanishing boundary conditions for the u -field and corresponding v -field of the Ito type equation: (a) \mathcal{PT} -symmetric case with $A = 3$, $c = 1$, $\alpha = -1/3$, $\beta = 1$ and $\gamma = -1/27^2$; (b) same values as in panel (a) for a single trajectory with $\zeta_0 = 0.04$; (c) broken \mathcal{PT} -symmetric case with $A \approx 3.054 - 0.783i$, $c = 1$, $\alpha = -1/3$, $\beta = 1 - i$ and $\gamma = -1/27^2 - i/2$.

We exclude the trivial solutions $A = B = A + B = 0$ as they all lead to $\kappa_2 = 0$. Solving (4.15) for this factorization gives

$$\zeta - \zeta_0 = \pm \frac{2}{(A - B)\sqrt{\lambda}} \left[\frac{\operatorname{arctanh}\left(\frac{\sqrt{v}}{\sqrt{B}}\right)}{\sqrt{B}} - \frac{\operatorname{arctanh}\left(\frac{\sqrt{v}}{\sqrt{A}}\right)}{\sqrt{A}} \right], \quad (4.25)$$

which reduces to (4.18) in the limit $B \rightarrow A$. Arguing as in the previous case, the real solutions are obtained from (4.18) for $\lambda > 0$ and $0 < v < A < B$. For other configurations of the ordering we replace in (4.25) the $\operatorname{arctanh}$ by arcoth when the argument becomes greater than one. For the same reasons as in the previous section we isolate v from this equation and obtain

$$v(\zeta) = A \tanh^2 \left[\frac{1}{2} \sqrt{\lambda} \sqrt{A} (B - A) (\zeta - \zeta_0) + \sqrt{\frac{A}{B}} \operatorname{arctanh} \left(\frac{\sqrt{v(\zeta)}}{\sqrt{B}} \right) \right]. \quad (4.26)$$

Simply by considering the functions on the right hand side of (4.26), we observe the asymptotic behaviour $\lim_{\zeta \rightarrow \pm\infty} v(\zeta) = A$. In this case the vanishing asymptotic boundary conditions for u can be implemented without additional constraints on the model defining parameters $\alpha, \beta, \gamma, \phi$. For other orderings of v, A, B we may also obtain $\lim_{\zeta \rightarrow \pm\infty} v(\zeta) = B$.

When $\lim_{\zeta \rightarrow \pm\infty} v(\zeta) = A$ all constraints in (4.16) and (4.21)-(4.24) are satisfied with the choice

$$A = \frac{c^2(\beta - 3\alpha)}{2\sqrt{3}\alpha^{3/2}\sqrt{-\beta}} \quad \text{and} \quad B = -\frac{c\sqrt{-\beta}}{\sqrt{3}\alpha^{3/2}}, \quad (4.27)$$

whereas when $\lim_{\zeta \rightarrow \pm\infty} v(\zeta) = B$ we need to exchange A and B in (4.27). For the solution reported in [43] the possible values for α, β, γ were restricted because the value of B was pre-selected, but as we have shown here this is not necessary.

Choosing vanishing boundary conditions we depict the real solutions in figure 32 for the different regimes and real initial values ζ_0 .

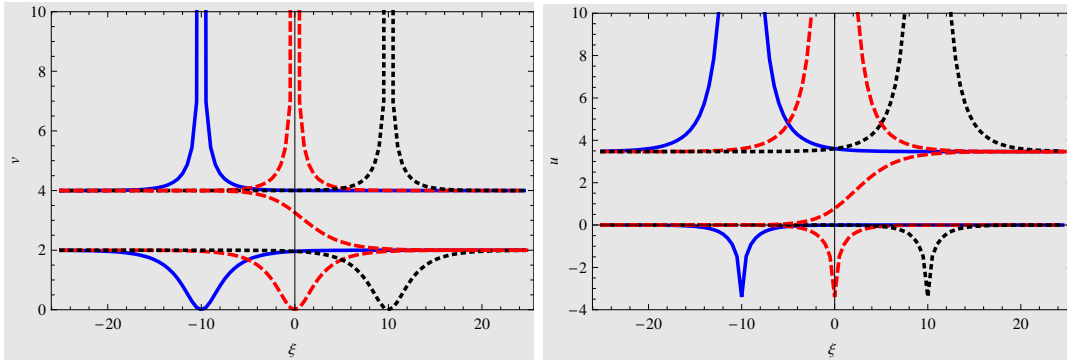


Figure 32: Soliton, kink and cusp type solutions for the Ito type equations with $\alpha = -\beta = 1/(2\sqrt{3})$, $\gamma = 1$, $c = -1$, $A = 2$ and $B = 4$. The initial values are takes to be $\zeta_0 = -10$ solid (blue), $\zeta_0 = 0$ dashed (red) and $\zeta_0 = -10$ dotted (black). (a) v -field; (b) u -field.

Our findings disagree slightly with those in [43], where the case $0 < v < |A| < |B|$ was reported to be of cusp type, whereas we observe that it is of a standard soliton nature. Our numerical findings are in agreement with the factorization of the right hand side of equation (4.13), which implies that $v_\zeta(0) = 0$ and not infinity as needed for a cusp solution. We also find a new kink type solution in the region $0 < |A| < v < |B|$ not reported by Kawamoto. In the regions $0 < v < A < B$ and $0 < A < B < v$ we observe explicitly the \mathcal{PT} -symmetry $\zeta \rightarrow -\zeta + 2\zeta_0$, $v \rightarrow v$ and $u \rightarrow u$.

Next we investigate some complex solutions by taking the initial values ζ_0 to be purely imaginary. For this type of the factorization the linearisation around the point A and B is straightforward as the square root in (4.15) can be taken. Parameterizing $A = r_A e^{i\theta_A}$, $B = r_B e^{i\theta_B}$ and $\lambda = r_\lambda e^{i\theta_\lambda}$ the eigenvalues of the Jacobian when linearized about $v = A$ are computed to

$$j_k = \pm \sqrt{r_A r_\lambda} \left[\cos \left(\frac{3\theta_A}{2} + \frac{\theta_\lambda}{2} \right) r_A - \cos \left(\frac{\theta_A}{2} + \theta_B + \frac{\theta_\lambda}{2} \right) r_B \right] \\ + i(-1)^k \sqrt{r_A r_\lambda} \left[\sin \left(\frac{3\theta_A}{2} + \frac{\theta_\lambda}{2} \right) r_A - \sin \left(\frac{\theta_A}{2} + \theta_B + \frac{\theta_\lambda}{2} \right) r_B \right] \quad (4.28)$$

for $k = 1, 2$. For the linearisation around $v = B$ we obtain (4.28) with $A \leftrightarrow B$.

By tuning our free parameters we can produce any desired characteristic behaviour for the fixed points at A and B . For instance in the \mathcal{PT} -symmetric setting for $A, B \in \mathbb{R}^+$ we

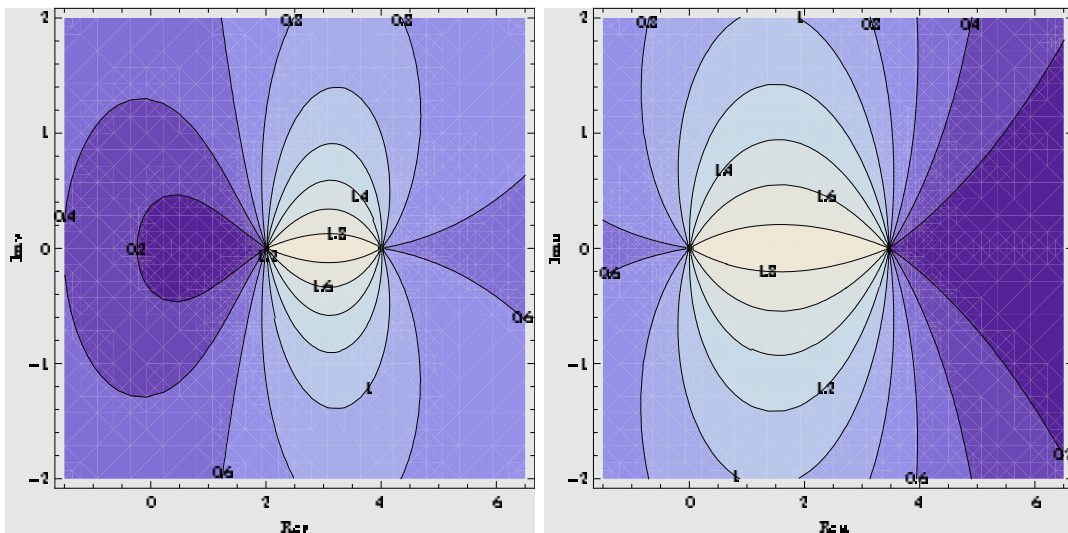


Figure 33: Complex asymptotically constant type II trajectories for the \mathcal{PT} -symmetric Ito type system for purely complex initial values ζ_0 with $\alpha = -\beta = 1/(2\sqrt{3})$, $\gamma = 1$, $c = -1$, $A = 2$ and $B = 4$. (a) v -field; (b) u -field.

always obtain two real degenerate eigenvalues when $\lambda \in \mathbb{R}^+$ and therefore star nodes at $v = A$ and $v = B$. In figure 33 we report an example of this type with $j_1 = j_2 = \mp 1/\sqrt{6}$.

We also observe in figure 33a that the complex trajectories surround the real solution with the asymptotic point or points in common. For instance, the trajectory with $\text{Im } \zeta_0 = 1$ corresponds to a complexified version of a real soliton solution in the regime $0 < v < A < B$ with asymptotic behaviour $\lim_{\zeta \rightarrow \pm\infty} v(\zeta) = A$. In the u -plane the real solution becomes a cusp solution running off to infinity, whereas the complex solutions close. We may also identify complexified versions of the kink solutions in the regime $0 < A < v < B$, such as for instance the trajectory with $\text{Im } \zeta_0 = 5$ in the v -plane with asymptotic behaviour $\lim_{\zeta \rightarrow +\infty} v(\zeta) = A$ and $\lim_{\zeta \rightarrow -\infty} v(\zeta) = B$. In the u -plane the qualitative behaviour remains the same with asymptotic behaviour $\lim_{\zeta \rightarrow -\infty} u(\zeta) = 0$ and $\lim_{\zeta \rightarrow \infty} u(\zeta) = -c/\alpha$. These features may also be derived analytically from (4.26). The reality of the energy is once more guaranteed by the symmetry $v^*(\zeta) = v(-\zeta)$ and $u^*(\zeta) = u(-\zeta)$.

Similarly as for the trigonometric solution of the KdV equation, by changing the parameters we can predict some periodic solutions. In the \mathcal{PT} -symmetric setting this is achieved for $A, B \in \mathbb{R}^+$ when taking $\lambda \in \mathbb{R}^-$, as in this case the two eigenvalues become purely complex and therefore the fixed point becomes a centre. For this type of solution this can be achieved either for the point $v = A$ or $v = B$. We depict an example of such solutions in figure 34 with eigenvalues $j_{1/2} = \pm i1/\sqrt{6}$. In the v -plane we observe that the complex trajectories encircle the points A or B whereas in the u -plane the trajectories surround the points $-c/\alpha$ and 0 for $\text{Im } \zeta_0 > 0$ or $\text{Im } \zeta_0 < 0$, respectively.

Again we observe the symmetry relations $v^*(\zeta) = v(-\zeta)$ and $u^*(\zeta) = u(-\zeta)$ ensuring the reality of the energy, but as for the trigonometric solution of the KdV equation we may compute the energy in this case explicitly. Taking the trajectories surrounding A in the

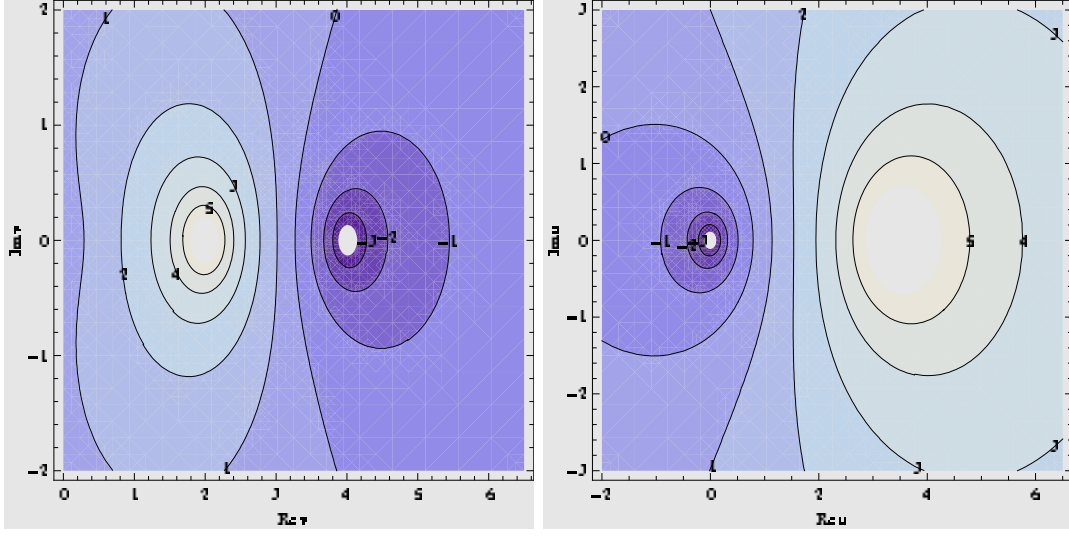


Figure 34: Complex periodic trajectories for type II \mathcal{PT} -symmetric Ito type system for purely complex initial values ζ_0 with $\alpha = -\beta = 1/(2\sqrt{3})$, $\gamma = -1$, $c = -1$, $A = 2$ and $B = 4$. (a) v -field; (b) u -field.

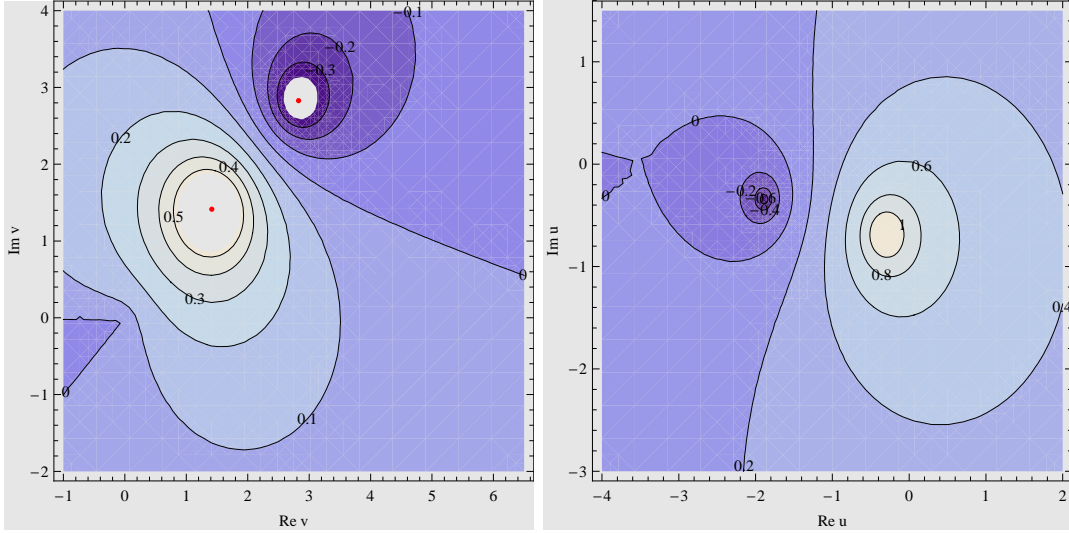


Figure 35: Complex periodic trajectories for type II broken \mathcal{PT} -symmetric Ito type system for purely complex initial values ζ_0 with $\alpha = 1/(2\sqrt{3})$, $\beta = \frac{(1-2i)+2\sqrt{-1-i}}{2\sqrt{3}}$, $\gamma = \frac{1}{48}(-i + \sqrt{-1-i})$, $c = -1$, $A = (1+i)\sqrt{2}$ and $B = (2+2i)\sqrt{2}$. (a) v -field; (b) u -field.

v -plane to be the contour Γ we compute

$$E_{T_A} = \oint_{\Gamma} \mathcal{H}[v(\zeta)] \frac{dv}{v_{\zeta}} = \oint_{\Gamma} \frac{\mathcal{H}[v]}{\sqrt{\lambda}\sqrt{v}(v-A)(v-B)} dv \quad (4.29)$$

$$= -\pi \frac{\sqrt{-\gamma\kappa_2}}{\alpha\sqrt{A}(A-B)} \left[cA^2 + \kappa_2 A + \frac{\beta}{3} \left(\frac{c}{\alpha} + \frac{\kappa_2}{\alpha A} \right)^3 \right]. \quad (4.30)$$

For the trajectories surrounding B in the v -plane we obtain in a similar way $E_{T_B} =$

$E_{T_A}(A \leftrightarrow B)$.

Considering the amount of free parameters we have at our disposal, the expression for (4.28) also suggests that we will be able to generate any type of fixed point even for the broken \mathcal{PT} -symmetric scenario. Most unexpected is probably that we may even generate periodic orbits in that case. For this to happen we require $3\theta_A + \theta_\lambda = \pi$ and $\theta_A + 2\theta_B + \theta_\lambda = \pi$ to hold. A solution to these equations, leading to the eigenvalues $j_{1/2} = \pm i2\sqrt{2}$, is presented in figure 35.

As already seen for the complex KdV-system in section 2.1.2, we can also break the \mathcal{PT} -symmetry in a more controlled way and restore the reality of the energy given by (4.30). Making for instance the parameter choice

$$\alpha = r_\alpha e^{-\frac{i}{2} \arctan\left(\frac{7}{4\sqrt{2}}\right)}, \quad \beta = 3r_\alpha e^{i\frac{\pi}{4}}, \quad \gamma = \mu \frac{\beta - \alpha}{\alpha}, \quad c = -1, \quad (4.31)$$

$$A = \frac{c(\beta - \alpha)}{2\sqrt{3}\alpha^{3/2}\sqrt{-\beta}}, \quad B = 2A, \quad (4.32)$$

with $\mu \in \mathbb{R}^+$ and $r_\alpha \in \mathbb{R}$ being unconstrained constants, we obtain for the energy of a periodic trajectory around the point A the real expression

$$E_{T_A} = -\frac{\pi}{3r_\alpha^2} \sqrt{\frac{5\mu}{3}}. \quad (4.33)$$

Notice that in this case we have two free parameters available allowing to tune the real energy together with the model, despite the fact that any of these the Hamiltonians is neither Hermitian nor \mathcal{PT} -symmetric. We depict an example for such type of trajectory in figure 36. We notice that the trajectories are qualitatively the same as those with complex energies depicted for instance in figure 35.

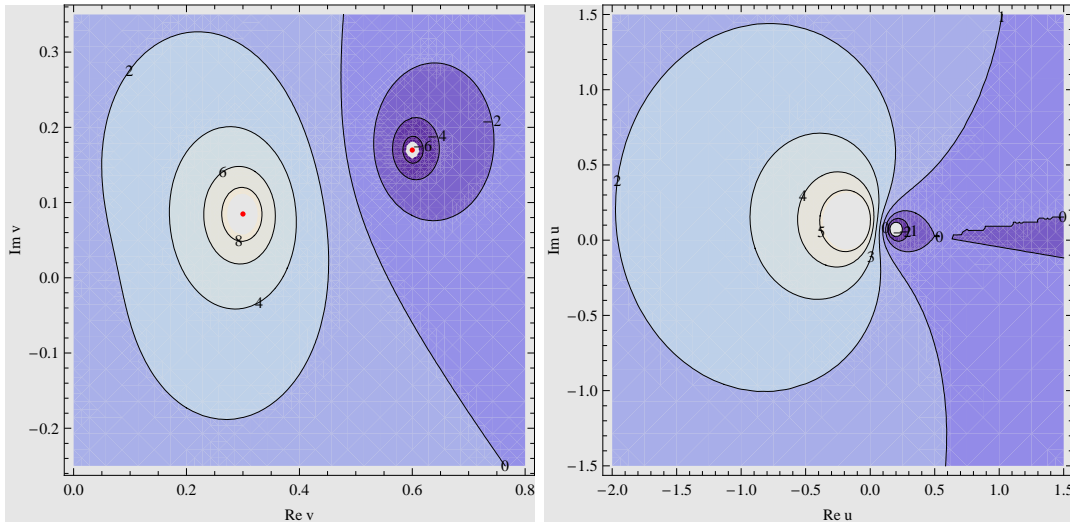


Figure 36: Complex periodic trajectories for type II broken \mathcal{PT} -symmetric Ito type system with real energy $E_{T_A} \approx -0.4275$ for purely complex initial values ζ_0 for the parameter choice in (4.31) and (4.32) with $r_\alpha = 2$ and $\mu = 2$; (a) v -field; (b) u -field.

4.1.3 Type III solutions

Next we assume that $R(v) = v(v - A)^2(B + v)(C + v)$, which is achievable upon the constraints

$$\begin{aligned}\kappa_1 &= \frac{(\beta - 2\alpha)c^2 + [A^2 + 2A(B + C) + BC]\alpha^3}{2\alpha^2}, \\ \kappa_2 &= \frac{A[2BC + A(B + C)]\alpha^3}{c(\beta - \alpha)}, \\ \kappa_3 &= \frac{[c^2 - [A^2 + 2(B + C)A + BC]\alpha^2]c}{2\alpha^2} - \frac{A(2A + B + C)[2BC + A(B + C)]\alpha^3}{2(\beta - \alpha)c} - \frac{\beta c^3}{3\alpha^3},\end{aligned}\tag{4.34}$$

$$A = -\frac{\sqrt{3}\sqrt{-\beta\alpha^3(\alpha - \beta)^2c^2BC(B + C)^2}}{\beta\alpha^3(B + C)^2} - \frac{2BC}{B + C}.$$

Now we have two free parameters at our disposal. In this case the solution of (4.15) leads to

$$\zeta - \zeta_0 = \pm \frac{2}{A\sqrt{B}\sqrt{\lambda}} \frac{1}{v} \left\{ F \left[\arcsin \left(\frac{\sqrt{B}}{\sqrt{v}} \right) \middle| \frac{C}{B} \right] + \Pi \left[\frac{A}{B}; -\arcsin \left(\frac{\sqrt{B}}{\sqrt{v}} \right) \middle| \frac{C}{B} \right] \right\}, \tag{4.35}$$

with $F[\phi|m]$ denoting an elliptic function of the first and $\Pi[n; \phi|m]$ an incomplete elliptic function.

Choosing B and C conveniently we compute some trajectories similarly as in the previous subsection and depict our results in figure 37.

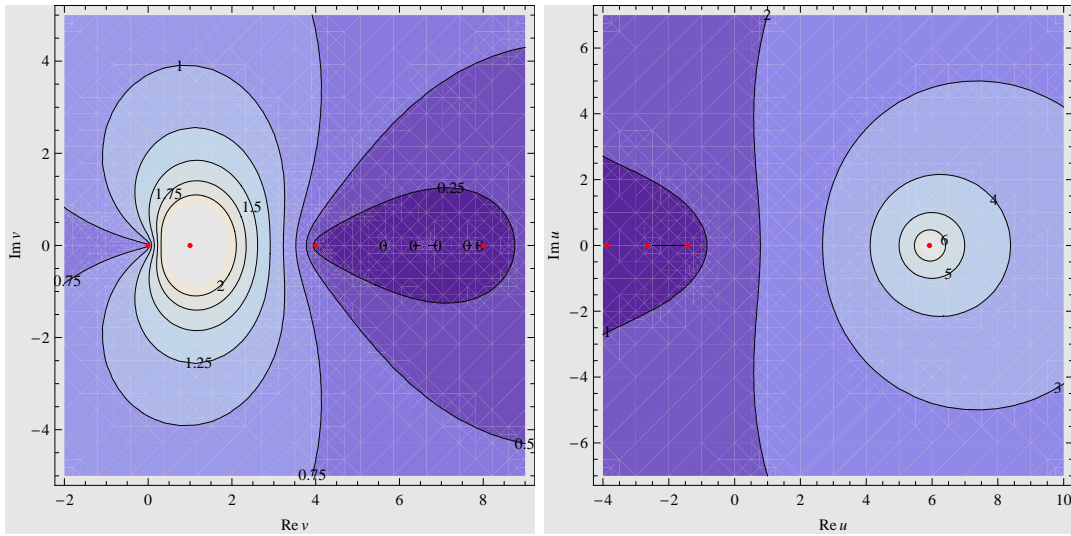


Figure 37: Complex periodic trajectories for the type III \mathcal{PT} -symmetric Ito type system for purely complex initial values ζ_0 with $\alpha = -\beta = 2\sqrt{6}/19$, $\gamma = -1$, $c = -1$, $A = 1$, $B = 4$ and $C = 8$.

We identify some trajectories surrounding the point A in the v -plane for which we

compute the energy as

$$E_{T_A} = \oint_{\Gamma} \mathcal{H}[v(\zeta)] \frac{dv}{v\zeta} = \oint_{\Gamma} \frac{\mathcal{H}[v]}{\sqrt{\lambda}\sqrt{(v-B)(v-C)v(v-A)}} dv \quad (4.36)$$

$$= \pi \frac{\sqrt{-\gamma\kappa_2}}{\alpha\sqrt{(A-B)(A-C)A}} \left[cA^2 + \kappa_2A + \frac{\beta}{3} \left(\frac{c}{\alpha} + \frac{\kappa_2}{\alpha A} \right)^3 \right]. \quad (4.37)$$

As seen for the type II solutions we may also in this case break the \mathcal{PT} -symmetry and still obtain periodic solutions. Moreover, we can break the symmetry further, that is also on the level of the Hamiltonian, and still render the expression for E_{T_A} real. Since in this case we have even an additional parameter C at our disposal it is conceivable that we might even have a free variable left in the expression for the real energy. We leave this question for a future investigation.

An example for broken \mathcal{PT} -symmetry is depicted in figure 38.

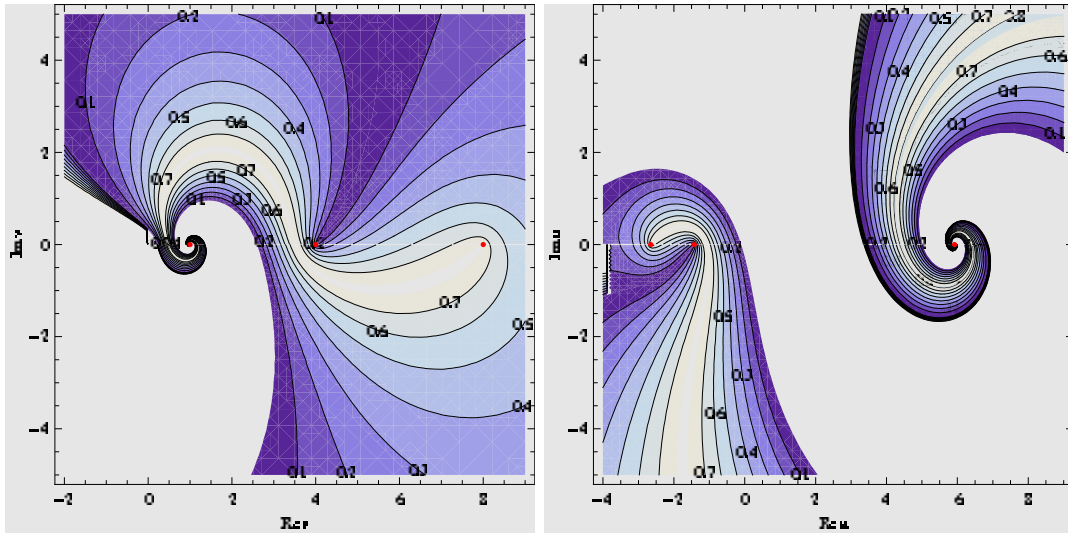


Figure 38: Complex periodic trajectories for the type III with broken \mathcal{PT} -symmetry for the Ito type system for purely complex initial values ζ_0 with $\alpha = -\beta = 2\sqrt{6}/19$, $\gamma = -1 + i$, $c = -1$, $A = 1$, $B = 4$ and $C = 8$.

5. \mathcal{PT} -symmetric deformations of the Ito type equations

Since the Hamiltonian \mathcal{H}_I admits the four different types of antilinear symmetries (4.5)-(4.8), we have now the options to apply the deformation maps δ_ε^+ and δ_ε^- introduced in (3.1) to the fields u and v in different combinations. Accordingly we define four different \mathcal{PT} -symmetric models with two deformation parameters ε, μ suitable normalized by the following Hamiltonian densities

$$\mathcal{H}_{\varepsilon, \mu}^{++} = -\frac{\alpha}{2}uv^2 - \frac{\beta}{6}u^3 - \frac{\gamma}{1+\varepsilon}(iu_x)^{\varepsilon+1} - \frac{\phi}{1+\mu}(iv_x)^{\mu+1}, \quad (5.1)$$

$$\mathcal{H}_{\varepsilon, \mu}^{+-} = \frac{\alpha}{1+\mu}u(iv)^{\mu+1} - \frac{\beta}{6}u^3 - \frac{\gamma}{1+\varepsilon}(iu_x)^{\varepsilon+1} + \frac{\phi}{2}v_x^2, \quad (5.2)$$

$$\mathcal{H}_{\varepsilon, \mu}^{-+} = -\frac{\alpha}{2}uv^2 - \frac{i\beta}{(1+\varepsilon)(2+\varepsilon)}(iu)^{2+\varepsilon} + \frac{\gamma}{2}u_x^2 - \frac{\phi}{1+\mu}(iv_x)^{\mu+1}, \quad (5.3)$$

$$\mathcal{H}_{\varepsilon, \mu}^{--} = \frac{\alpha}{1+\mu}u(iv)^{\mu+1} - \frac{i\beta}{(1+\varepsilon)(2+\varepsilon)}(iu)^{2+\varepsilon} + \frac{\gamma}{2}u_x^2 + \frac{\phi}{2}v_x^2. \quad (5.4)$$

By construction we have $\mathcal{PT}_{ij} : \mathcal{H}_{\varepsilon, \mu}^{ij} \mapsto \mathcal{H}_{\varepsilon, \mu}^{ij}$ with $i, j \in \{+, -\}$ and $\lim_{\varepsilon, \mu \rightarrow 1} \mathcal{H}_{\varepsilon, \mu}^{ij} = \mathcal{H}_I$. The corresponding equations of motion resulting from (4.4) are

$$\begin{aligned} \mathcal{H}_{\varepsilon, \mu}^{++} : u_t + \alpha vv_x + \beta uu_x + \gamma u_{xxx, \varepsilon} &= 0, & \mathcal{H}_{\varepsilon, \mu}^{+-} : u_t + \alpha v_\mu v_x + \beta uu_x + \gamma u_{xxx, \varepsilon} &= 0, \\ v_t + \alpha (uv)_x + \phi v_{xx, \mu} &= 0, & v_t + \alpha (uv_\mu)_x + \phi v_{xx} &= 0, \end{aligned} \quad (5.5)$$

$$\begin{aligned} \mathcal{H}_{\varepsilon, \mu}^{-+} : u_t + \alpha vv_x + \beta u_\varepsilon u_x + \gamma u_{xxx} &= 0, & \mathcal{H}_{\varepsilon, \mu}^{--} : u_t + \alpha v_\mu v_x + \beta u_\varepsilon u_x + \gamma u_{xxx} &= 0, \\ v_t + \alpha (uv)_x + \phi v_{xx, \mu} &= 0, & v_t + \alpha (uv_\mu)_x + \phi v_{xxx} &= 0. \end{aligned} \quad (5.6)$$

Naturally there exist also possibilities to construct non-Hamiltonian deformations. Noting for instance that the first equation related to $\mathcal{H}_{\varepsilon, \mu}^{++}$ is also invariant under \mathcal{PT}_{+-} we may combine it with the second equation resulting from $\mathcal{H}_{\varepsilon, \mu}^{+-}$ and define the \mathcal{PT}_{+-} -invariant system

$$\begin{aligned} u_t + \alpha vv_x + \beta uu_x + \gamma u_{xxx, \varepsilon} &= 0, \\ v_t + \alpha (uv_\mu)_x + \phi v_{xx} &= 0. \end{aligned} \quad (5.7)$$

We have now numerous new physically feasible theories to be investigated. Here we will only present few examples. Having two parameters at our disposal allows to obtain more analytic expressions for the solutions. Technically we have two problems to overcome. First of all we have to decouple the equations and subsequently carry out all the integrations. In order to achieve the first aim we focus mainly on the case $\phi = 0$ as this will allow to express u in terms of v in a simple manner. This choice will eliminate the deformation term in $\mathcal{H}_{\varepsilon, \mu}^{++}$ and we therefore concentrate here on $\mathcal{H}_{\varepsilon, \mu}^{+-}$ to study the interplay between the two parameters.

5.1 The model $\mathcal{H}_{\varepsilon, \mu}^{+-}(\alpha, \beta, \gamma, u, v)$

As a further simplification we set the constant κ_2 to zero, which results in the first integration of the equation for v_t . We may then integrate again and obtain a decoupled equation solely involving the field u

$$u_\zeta^{\varepsilon+1} = i^{1-\varepsilon} \frac{\varepsilon+1}{\gamma\varepsilon} \left[\kappa_3 + \kappa_1 u + \frac{c}{2}u^2 - \frac{\beta}{6}u^3 + \frac{\alpha}{2} \frac{1-\mu}{1+\mu} \left(\frac{\alpha}{c} \right)^{\frac{1+\mu}{1-\mu}} u^{\frac{2}{1-\mu}} \right], \quad (5.8)$$

with the two fields related as

$$u = \frac{c}{\alpha}(iv)^{1-\mu}. \quad (5.9)$$

To be able to carry out the final integration in (5.8) we would like the right hand side to acquire the form of a factorizable polynomial in u . This is possible for several specific choices and with the additional choice of ε we may even construct analytic solutions.

$$\mathcal{H}_{\varepsilon,1/3}^{+-}(\alpha, \beta, \gamma, u, v)$$

This case is entirely reducible to the deformation of the KdV $\mathcal{H}_{\varepsilon}^{+}(\beta, \gamma, u)$ when noticing that

$$\mathcal{H}_{\varepsilon}^{+}\left(\beta - \frac{3\alpha^3}{2c^2}, \gamma \frac{2\varepsilon}{1+\varepsilon} i^{\varepsilon-1}, u\right) = \mathcal{H}_{\varepsilon,1/3}^{+-}\left[\alpha, \beta, \gamma, u, \left(\frac{\alpha}{\beta}u\right)^{3/2}\right]. \quad (5.10)$$

where we used the relation between u and v as specified in (5.9) for $\mu = 1/3$.

$$\mathcal{H}_{-1/2,1/2}^{+-}$$

The choice $\mu = 1/2$ converts the right hand side of (5.8) into a fourth order polynomial. Let us next assume the factorization is of the form $\lambda(u - A)^2(u - B)^2$, which is indeed possible if the following constraints hold

$$\lambda = \frac{e^{-i\pi/4}\alpha^4}{6c^3\gamma}, \quad \kappa_1 = \frac{c^6\beta^3 - 12c^4\alpha^4\beta}{48\alpha^8}, \quad \kappa_3 = \frac{c^5(c^2\beta^2 - 12\alpha^4)^2}{384\alpha^{12}}, \quad (5.11)$$

$$A = \frac{c^3\alpha^4\beta \pm \sqrt{3}\sqrt{c^6\alpha^8\beta^2 - 8c^4\alpha^{12}}}{4\alpha^8}, \quad B = \frac{c^3\beta\alpha^4 \mp \sqrt{3}\sqrt{c^6\alpha^8\beta^2 - 8c^4\alpha^{12}}}{4\alpha^8}. \quad (5.12)$$

Notice that all the free parameters are fixed in this case, as a consequence of having already pre-selected $\kappa_2 = 0$. We analyse this model in figure 39.

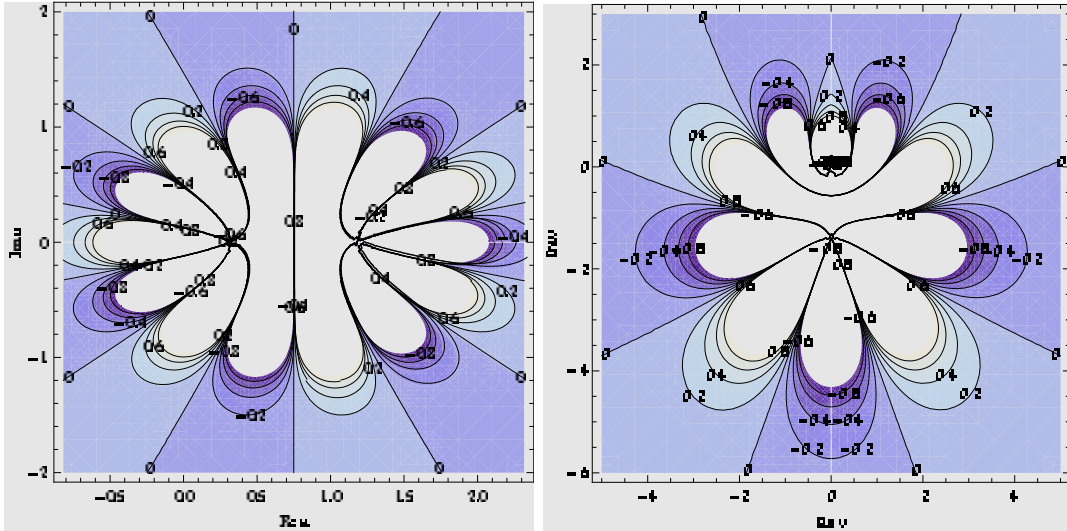


Figure 39: Complex periodic trajectories for the \mathcal{PT}_{+-} -symmetric system $\mathcal{H}_{-1/2,1/2}^{+-}$ for purely complex initial values ζ_0 with $\alpha = 1, \beta = 3, \gamma = 1, c = 1, A = (3 - \sqrt{3})/4$ and $B = (3 + \sqrt{3})/4$.

We observe that the \mathcal{PT}_{+-} -symmetry manifests itself now through $v^*(\zeta) = -v(-\zeta)$ and $u^*(\zeta) = u(-\zeta)$. Furthermore we recognise that the asymptotic limits of the u -field are A and B .

Of course there are plenty more models one may explore.

5.2 The non-Hamiltonian deformation (5.7)

Let us briefly comment on one of the possibilities to construct deformations of non-Hamiltonian systems (5.7). We consider again the case $\phi = 0$ and $\kappa_2 = 0$ and integrate the first equation in (5.7) for $\varepsilon = 1$ and $\mu \neq 3$

$$u_\zeta^2 = \frac{2}{\gamma} \left[\kappa_3 + \kappa_1 u + \frac{c}{2} u^2 - \frac{\beta}{6} u^3 + \frac{\alpha}{2} \left(\frac{c}{\alpha} \right)^{\frac{2}{\mu-1}} \frac{1-\mu}{3-\mu} u^{\frac{3-\mu}{1-\mu}} \right]. \quad (5.13)$$

The v -field is related to the u -field via (5.9). The boundary conditions have to be treated by distinguishing different case. For instance, when $(3 - \mu)/(1 - \mu) \geq 0$ the vanishing asymptotic boundary conditions for u and its derivatives demand that $\kappa_1 = \kappa_3 = 0$.

The simplest case to consider is $\mu = -1$, which is just the KdV-system with a re-defined speed of the wave $c \rightarrow c + \alpha^2/c$.

A further simple example is to take $\mu = 1/3$ for which we can find an explicit solution $u(\zeta)$. The right hand side of (5.13) can be factorized into $\lambda(u - A)^2(u - B)^2$ with

$$\lambda = \frac{c^3}{4\alpha^2\gamma}, \quad \kappa_1 = \frac{\alpha^4\beta^3 - 9c^4\alpha^2\beta}{27c^6}, \quad \kappa_3 = \frac{(\alpha^3\beta^2 - 9c^4\alpha)^2}{162c^9}, \quad (5.14)$$

$$A = \frac{c^3\alpha^2\beta - \sqrt{3}\sqrt{c^6\alpha^4\beta^2 - 6c^{10}\alpha^2}}{3c^6}, \quad B = \frac{\alpha^2\beta c^3 + \sqrt{3}\sqrt{c^6\alpha^4\beta^2 - 6c^{10}\alpha^2}}{3c^6}. \quad (5.15)$$

for which (5.13) can be integrated further and solved for u . We find

$$u(\zeta) = \frac{Be^{\pm A(\zeta-\zeta_0)\sqrt{\lambda}} - Ae^{\pm B(\zeta-\zeta_0)\sqrt{\lambda}}}{e^{\pm A(\zeta-\zeta_0)\sqrt{\lambda}} - e^{\pm B(\zeta-\zeta_0)\sqrt{\lambda}}} \quad \text{and} \quad v(\zeta) = -i \left(\frac{\alpha u(\zeta)}{c} \right)^{3/2}. \quad (5.16)$$

The system is easily linearized and qualitatively we find a similar behaviour as for the Hamiltonian systems, which we will, however, not present here in more detail. Thus, even though it is less clear how the \mathcal{PT} -symmetry can be utilized, we find that they are not fundamentally different from the Hamiltonian systems.

6. Conclusions

The main focus of this paper was to investigate the effects of \mathcal{PT} -symmetry and its breaking in complex nonlinear wave equations. In general we find that unlike as claimed for orbits in quantum mechanical one particle models [10, 11, 12, 13], trajectories in the complex plane of the field of a \mathcal{PT} -symmetric nonlinear system are not fundamentally distinct from those associated to systems with spontaneously or completely broken \mathcal{PT} -symmetry. Just from the general type of trajectory one can not conclude which type of setting one is considering. Of course invoking the information on the symmetry one can identify on this basis the \mathcal{PT} -symmetric case over the broken ones. However, based on this criterium the spontaneously broken cases are indistinguishable from the completely broken ones. This behaviour extends to the type of fixed points one may find. We observed that essentially

all types of fixed points, except saddle points, may occur, irrespective of the \mathcal{PT} -symmetry properties of the model. When identifying and varying certain constants of the model as bifurcation parameter the fixed point may undergo a Hopf bifurcation.

It appears that the entire phase space is filled out in the broken case, thus suggesting a chaotic behaviour. However, from the Poincaré-Bendixson theorem¹ we know that for a closed bounded and connected region in two dimensions this is impossible to occur.

The nature of the fixed points also indicates that the models are not Hamiltonian in the real and imaginary part of u , as only saddle points and centres would emerge in that case, whereas we found different types of fixed points and the absence of saddle points.

With regard to the energies we confirmed that fully \mathcal{PT} -symmetric systems have real energies, which could be calculated explicitly in many cases. When breaking this symmetry spontaneously by complexifying some free parameters in the solutions we obtained complex energies. As expected, the models related to the complex conjugates of these parameters have complex conjugate energies. More surprising are the findings obtained in various models that one may regain the reality of the energy by breaking the symmetry further. For the type III solutions of the Ito type systems it is conceivable the one might have free parameters in the expressions for the energy even when fixing the model. We conjecture that these models possess a different kind of antilinear symmetry yet to be identified.

We found that complex \mathcal{PT} -symmetric soliton solutions behave similarly as their real counterparts, albeit in the complex plane. The one-solitons travel in the complex plane while maintaining their overall shape and the two-soliton solution can be associated to two separate one-soliton solutions in the distant past and future. However, when the \mathcal{PT} -symmetry is broken the nature of the one-soliton solution changes into a breather, which only regains its shape after it has traveled a certain time and distance. The two-soliton solutions for this case can also be separated into these breathers in the distant past and future. The energy of the two-soliton solution was found to be the sum of the energies of the constituent one-soliton solutions in all scenarios. It would be interesting to investigate these features also for N-soliton solutions for $N > 2$ and different types of systems, such as the Ito type.

Besides guaranteeing the reality of the energy, \mathcal{PT} -symmetry was noted to be useful for various other reasons. We found that the symmetry allows for a natural " ε -prescription" to facilitate the computation of the energies in the complex plane by means of the Cauchy theorem. Identifying the different types of \mathcal{PT} -symmetries it also allows to formulate new physically feasible models with real energies. This procedure constitutes a natural and more general framework for some models which have already been known before, such as the generalized KdV-equations with the modified one as a special case.

Since many of the models discussed here are integrable, it is worth mentioning that most of the analysis carried out here for the Hamiltonian may also be performed for other conserved quantities of the same order in the fields having the same type of symmetry property. For some of the charges this is in fact not the case. Although in many deformed

¹**Poincaré-Bendixson Theorem:** *Let φ_t be a flow for a two dimensional dynamical systems and let \mathcal{D} be a closed, bounded and connected set $\mathcal{D} \in \mathbb{R}^2$, such that $\varphi_t(\mathcal{D}) \subset \mathcal{D}$ for all time. Furthermore \mathcal{D} does not contain any fixed point. Then there exists at least one limit cycle in \mathcal{D} .*

cases the question of integrability has not yet been answered decisively, the statement also holds for the lowest charges which are certain to exist.

The main difference between the deformed models and their undeformed counterparts is in general the occurrence of more and more Riemann sheets with increasing integer value for ε . We showed that in many cases non-integer values and even negative values for ε give rise to interesting solvable models. The overall structure of the trajectories and the nature of the fixed points is not fundamentally different, except that they usual extend over several Riemann sheets. Clearly we only presented here a limited number of solutions and many cases still need to be explored, especially for the second type of deformation for which even the factorization of the $P(u)$ -function remains an open issue.

When comparing the Ito type system with the KdV system we note that the former is not simply an add on to the latter, but gives rise to more complex structures. We found even for the undeformed case some new solutions such as those of kink type hitherto not reported. We also pointed out some minor discrepancies when compared to the literature. With regard to the deformations, which are all entirely new proposals, the conclusions are similar as for the deformed KdV-case. The major difference is that the interplay between the two deformation parameters allows for even more possibilities. Also in this case many possibilities remain unexplored.

As indicated at the end of section 2.1.3 and 3.1.3 we can obtain simple quantum mechanical systems as special cases from our analysis. For instance, the archetype deformation of the harmonic oscillator Hamiltonian $H = p^2 + x^2(ix)^\varepsilon$ can be obtained in various ways via the identification for the traveling wave $u \rightarrow x$ and $\zeta \rightarrow t$. As discussed, the deformed models $\mathcal{H}_\varepsilon^-$ yield precisely the quantum mechanical model with potential $V(x) = x^2(ix)^\varepsilon$, of which some cases were studied in [45]. From the models presented here there are more possibilities to arrive at such potential, as for instance also the non-Hamiltonian models (5.7) give rise to such type of potentials as may be seen from (5.13). Exploiting these observations allows to obtain many solutions and properties of these systems easily from our analysis overlooked up to now. Obviously, one may also construct new interesting quantum mechanical models in this way which have not been investigated so far.

In addition, this opens up immediately the more general question of studying properties of these systems as continuous functions of ε , rather than selecting just certain specific values as in this manuscript. Building for instance on the analogy with the potential systems should certainly reveal fundamentally different kinds of behaviour in some regions, such that for instance $\mathcal{H}_\varepsilon^-$ will probably have a qualitatively different behaviour for negative values of ε . We leave these type of questions for future investigations.

Clearly it would be very interesting to extend these type of analysis to other non-linear field equations such as Burgers, Bussinesque, KP, generalized shallow water equations, extended KdV equations with compacton solution, etc.

Acknowledgments: AF would like to thank the UGC Special Assistance Programme in the Applied Mathematics Department of the University of Calcutta and S.N. Bose National Centre for Basic Sciences for providing infrastructure and financial support. AC is supported by a City University Research Fellowship.

A. The ten similarity classes for J

For convenience we recall here the ten different similarity classes characterizing the fixed points of a two dimensional linear system (2.9) by the eigenvalues j_1 and j_2 of the Jacobian matrix J at the fixed point.

$j_i \in \mathbb{R}$	$j_1 > j_2 > 0$	unstable node
	$j_2 < j_1 < 0$	stable node
	$j_2 < 0 < j_1$	saddle point
$j_1 = j_2$, diagonal J	$j_i > 0$	unstable star node
	$j_i < 0$	stable star node
$j_1 = j_2$, nondiagonal J	$j_i > 0$	unstable improper node
	$j_i < 0$	stable improper node
$j_i \in \mathbb{C}$	$\text{Re } j_i > 0$	unstable focus
	$\text{Re } j_i = 0$	centre
	$\text{Re } j_i < 0$	stable focus

Table 1: Nature of a fixed point as classified by the eigenvalues of the Jacobian.

References

- [1] W. Heisenberg, Die beobachtbaren Größen in der Theorie der Elementarteilchen, *Zeit. für Physik* **120**, 513–538 (1943).
- [2] R. J. Eden, P. V. Landshoff, D. I. Olive, and J. C. Polkinghorne, *The Analytic S-matrix*, Cambridge University Press (1966).
- [3] I. Rotter, A non-Hermitian Hamilton operator and the physics of open quantum systems, *J. Phys.* **A42**, 153001(51) (2009).
- [4] C. M. Bender and S. Boettcher, Real Spectra in Non-Hermitian Hamiltonians Having PT Symmetry, *Phys. Rev. Lett.* **80**, 5243–5246 (1998).
- [5] C. M. Bender, Making sense of non-Hermitian Hamiltonians, *Rept. Prog. Phys.* **70**, 947–1018 (2007).
- [6] A. Mostafazadeh, Pseudo-Hermitian Representation of Quantum Mechanics, *Int. J. Geom. Meth. Mod. Phys.* **7**, 1191–1306 (2010).
- [7] P. Assis, *Non-Hermitian Hamiltonians in Field Theory*, VDM Verlag Dr. Müller, Saarbrücken (2010).
- [8] C. E. Rüter, R. Makris, K.G. and El-Ganainy, D. N. Christodoulides, M. Segev, and D. Kip, Observation of parity-time symmetry in optics, *Nature Physics* **6**, 192–195 (2010).
- [9] M. Fagotti, C. Bonati, D. Logoteta, P. Marconcini, and M. Macucci, Armchair graphene nanoribbons: PT-symmetry breaking and exceptional points without dissipation, arXiv:1102.2129v1 [cond-mat.mes-hall] .
- [10] A. Nanayakkara, Classical trajectories of 1D complex non-Hermitian Hamiltonian systems, *J. Phys.* **A37**, 4321–4334 (2004).

- [11] C. M. Bender, D. D. Holm, and D. W. Hook, Complex Trajectories of a Simple Pendulum, *J. Phys.* **A40**, F81–F90 (2007).
- [12] C. M. Bender, D. C. Brody, and D. W. Hook, Quantum effects in classical systems having complex energy, *J. Phys.* **A41**, 352003 (2008).
- [13] C. M. Bender, D. W. Hook, and K. S. Kooner, Classical Particle in a Complex Elliptic Potential, *J. Phys.* **A43**, 165201 (2010).
- [14] C. M. Bender, D. D. Holm, and D. W. Hook, Complexified Dynamical Systems, *J. Phys.* **A40**, F793–F804 (2007).
- [15] C. M. Bender, J. Feinberg, D. W. Hook, and D. J. Weir, Chaotic systems in complex phase space, *Pramana J. Phys.* **73**, 453–470 (2009).
- [16] A. Fring, A note on the integrability of non-Hermitian extensions of Calogero-Moser-Sutherland models, *Mod. Phys. Lett.* **21**, 691–699 (2006).
- [17] A. Fring and M. Znojil, *PT*-Symmetric deformations of Calogero models, *J. Phys.* **A40**, 194010(17) (2008).
- [18] P. E. G. Assis and A. Fring, From real fields to complex Calogero particles, *J. Phys.* **A42**, 425206(14) (2009).
- [19] A. Fring and M. Smith, Antilinear deformations of Coxeter groups, an application to Calogero models, *J. Phys.* **A43**, 325201(28) (2010).
- [20] C. M. Bender and D. W. Hook, Tunneling in classical mechanics, preprint arXiv:1011.0121 .
- [21] C. M. Bender and T. Arpornthip, Conduction bands in classical periodic potentials, *Pramana J. Phys.* **73**, 259–268 (2009).
- [22] C. M. Bender, D. W. Hook, P. N. Meisinger, and Q.-h. Wang, Complex Correspondence Principle, *Phys. Rev. Lett.* **104**, 061601 (2010).
- [23] C. M. Bender, D. C. Brody, J. Chen, and E. Furlan, *PT*-symmetric extension of the Korteweg-de Vries equation, *J. Phys.* **A40**, F153–F160 (2007).
- [24] A. Fring, *PT*-Symmetric deformations of the Korteweg-de Vries equation, *J. Phys.* **A40**, 4215–4224 (2007).
- [25] B. Bagchi and A. Fring, *PT*-symmetric extensions of the supersymmetric Korteweg-De Vries equation, *J. Phys.* **A41**, 392004(9) (2008).
- [26] C. M. Bender and J. Feinberg, Does the complex deformation of the Riemann equation exhibit shocks?, *J. Phys.* **A41**, 244004 (2008).
- [27] T. L. Curtright and D. B. Fairlie, Euler Incognito, *J. Phys.* **A41**, 244009 (2008).
- [28] C. M. Bender, F. Cooper, A. Khare, B. Mihaila, and A. Saxena, Compactons in *PT*-symmetric generalized Korteweg-de Vries Equations, *Pramana J. Phys.* **73**, 375–385 (2009).
- [29] P. E. G. Assis and A. Fring, Compactons versus Solitons, *Pramana J. Phys.* **74**, 857–865 (2010).
- [30] E. Wigner, Normal form of antiunitary operators, *J. Math. Phys.* **1**, 409–413 (1960).
- [31] E. Ergun and M. Saglam, On the Metric of a non-Hermitian Model, *Rep. on Math. Phys.* **65**, 367–378 (2010).

- [32] B. Fuchssteiner, The Lie algebra structure of degenerate Hamiltonian and bi-Hamiltonian systems, *Progr. Theor. Phys.* **68**, 1082–1104 (1982).
- [33] W. Oevel, On the integrability of the Hirota-Satsuma system, *Phys. Lett.* **A94**, 404–407 (1983).
- [34] L. Yang, K. Yang, and H. Luo, Complex version KdV equation and the periods solution, *Phys. Lett.* **A267**, 331–334 (2000).
- [35] W. I. Fushchych, N. I. Serov, and T. K. Ahmerov, On the conditional symmetry of the generalized KdV equation, *Rep. Ukr. Acad. Sci.* **12**, 28 (1991).
- [36] D. K. Arrowsmith and C. Place, *Dynamical Systems*, Chapman and Hall, London (1992).
- [37] B. Bagchi, S. Das, and A. Ganguly, New exact solutions of a generalized shallow water wave equation, *Physica Scripta* **82**, 025003 (2010).
- [38] R. Hirota, *The Direct Method in Soliton Theory*, CUP (2004).
- [39] A. Fring, P. R. Johnson, M. A. C. Kneipp, and D. I. Olive, Vertex operators and soliton time delays in affine Toda field theory, *Nucl. Phys.* **B430**, 597–614 (1994).
- [40] R. Hirota and J. Satsuma, Soliton solutions of a coupled Korteweg-de Vries equation, *Phys. Lett.* **A85**, 407–408 (1981).
- [41] J. Satsuma and R. Hirota, A coupled KdV Equation is one case of the Four-Reduction of the KP Hierachy, *J. Phys. Soc. Jap.* **51**, 3390–3397 (1982).
- [42] M. Ito, Symmetries and conservation laws of a coupled nonlinear wave equation, *Phys. Lett.* **A91**, 335–338 (1982).
- [43] S. Kawamoto, Cusp Soliton Solutions of the Ito-Type Coupled Nonlinear Wave Equation, *J. of the Phys. Soc. of Japan* **53**, 1203–1205 (1984).
- [44] C. Guha-Roy, B. Bagchi, and D. Sinha, Traveling-wave solutions and the coupled Korteweg de Vries equation, *J. Math Phys.* **27**, 2558–2561 (1986).
- [45] A. G. Anderson, C. M. Bender, and U. I. Morone, Periodic orbits for classical particles having complex energy, arXiv:1102.4822.

